

PSI Center for Neutron and Muon Sciences

ETH zürich

X-ray spectroscopy of light muonic atoms

with metallic magnetic calorimeters

Katharina von Schoeler

Trento, 14 October 2026

Our muon source

High Intensity Proton Accelerator

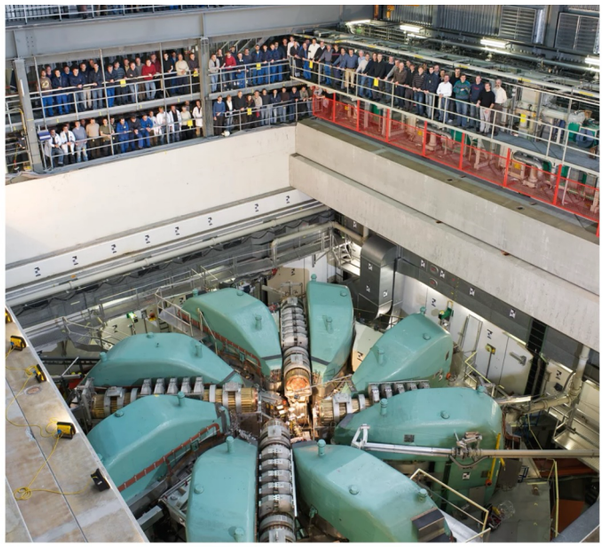

Muonic atoms

and their spectroscopy

Muonic atom spectroscopy

1. Stop muons in target material

2. Atomic capture in high principal quantum number n

3. Cascade down to the ground state via
   → Auger electron emission (dominating at high n)
   → characteristic x-ray emission (dominating at low n)
      → few keV to MeV range

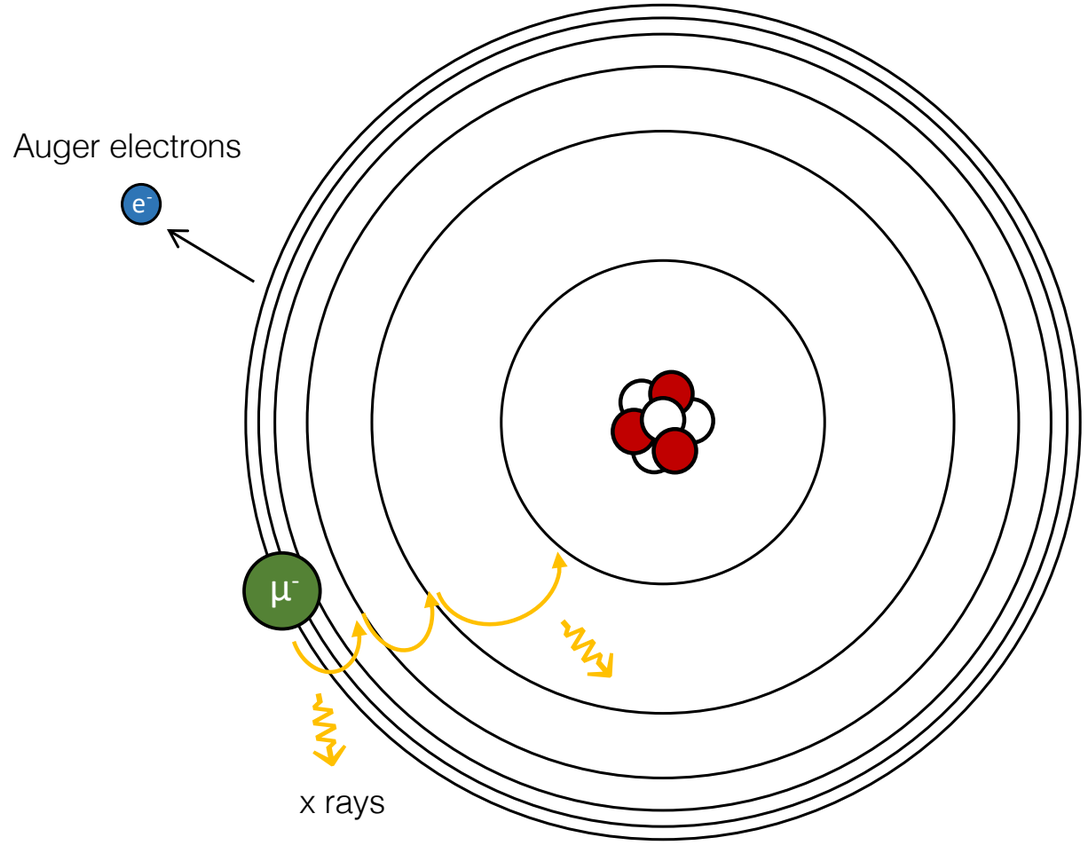

Muonic atom spectroscopy

1. Stop muons in target material

2. Atomic capture in high principal quantum number n

3. Cascade down to the ground state via
   → Auger electron emission (dominating at high n)
   → characteristic x-ray emission (dominating at low n)
      → few keV to MeV range

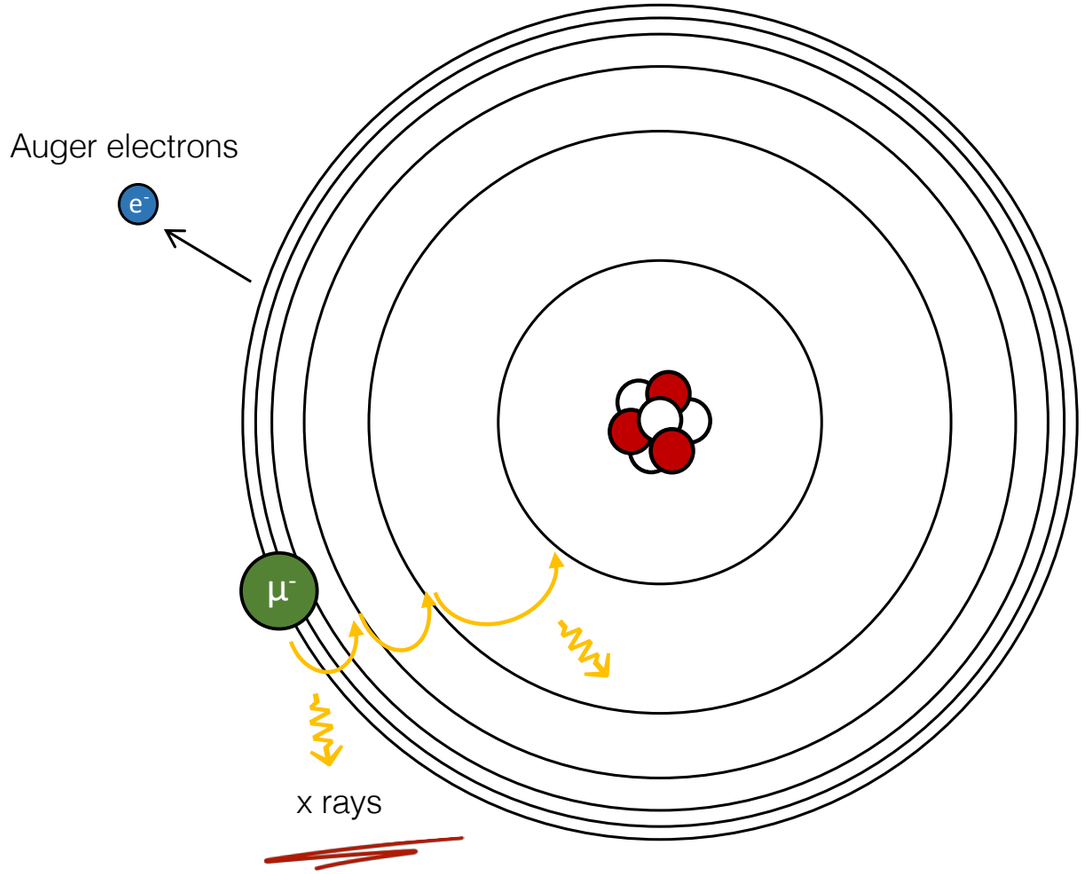

Muonic atom spectroscopy

1. Stop muons in target material

2. Atomic capture in high principal quantum number n

3. Cascade down to the ground state via
   → Auger electron emission (dominating at high n)
   → characteristic x-ray emission (dominating at low n)
      → few keV to MeV range

4. Decay in orbit (→ Michel electrons) or nuclear capture $\mu^- + (A,Z) \rightarrow (A, Z-1)^* + \nu_\mu$

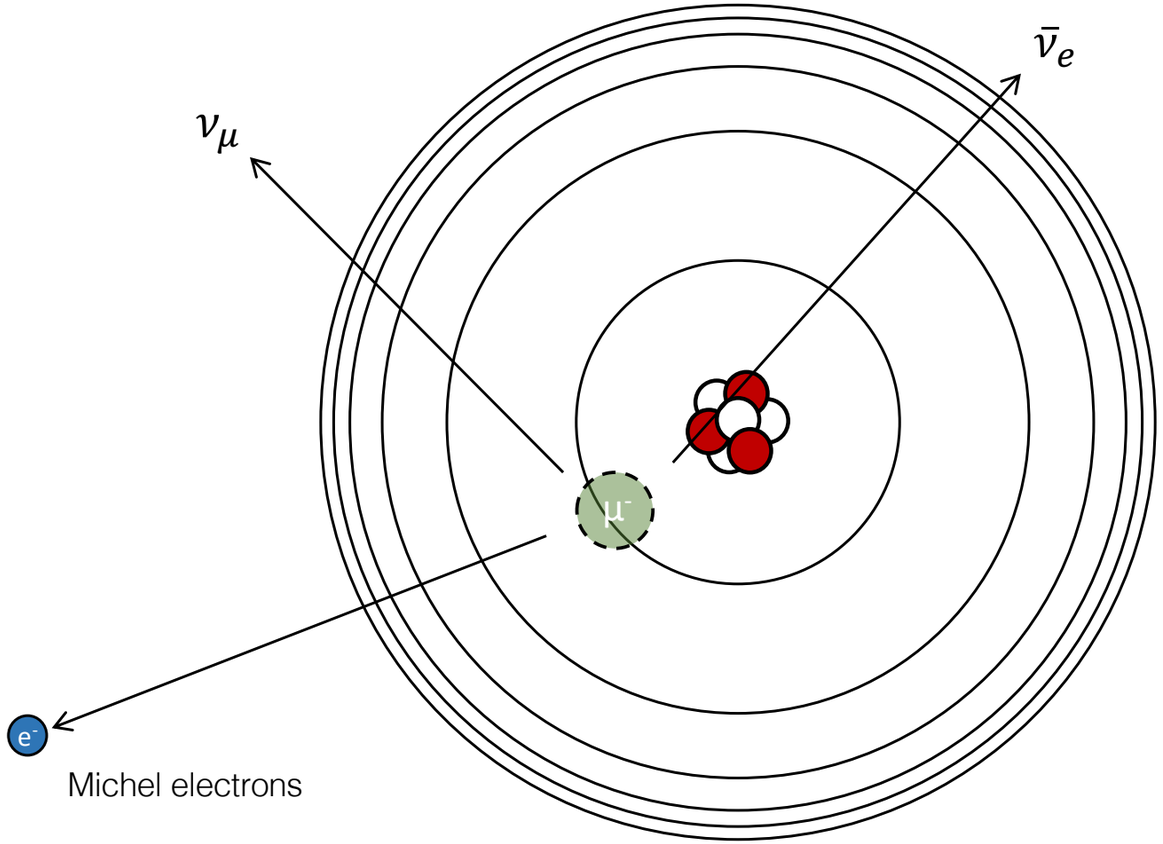

Finite nuclear size effect in muonic atoms

Muon mass: $m_\mu \approx 200 \cdot m_e$

Bohr radii: $r \propto \frac{n^2}{Z} \cdot \frac{1}{m}$ → 200 times smaller than ordinary atom

Finite nuclear size effect: $\delta E_{FNS}(n, \ell) = \frac{2(Z\alpha)^4}{3n^3} m^3 \langle r_c^2 \rangle \, \delta_{l0}$

→ Enhanced by 10^7!

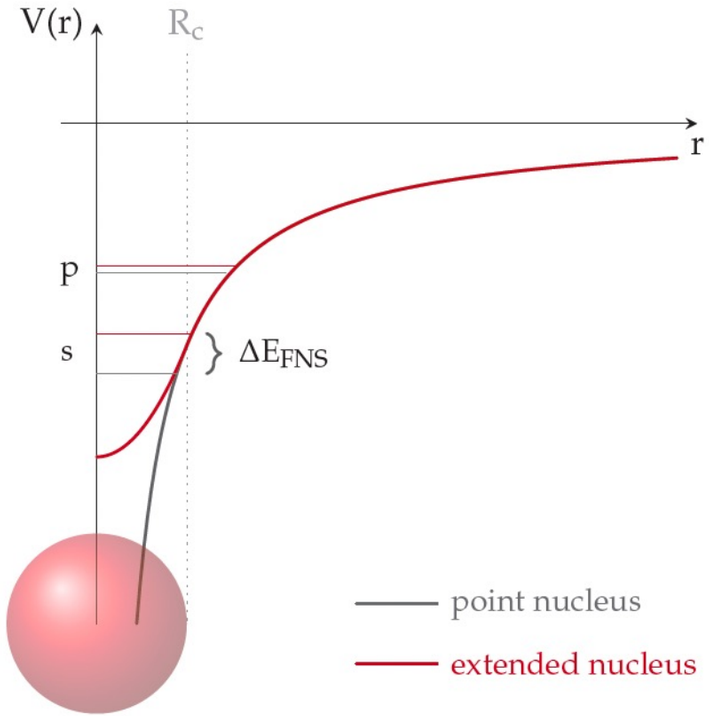

measure → theoretical model → extract

Transition energies → $E = E_{Dirac} + \delta E_{QED} + \delta E_{FNS}(\langle r_c^2 \rangle) + \delta E_{TPE}$ → Absolute $\langle r_c^2 \rangle$

Muonic atom spectroscopy

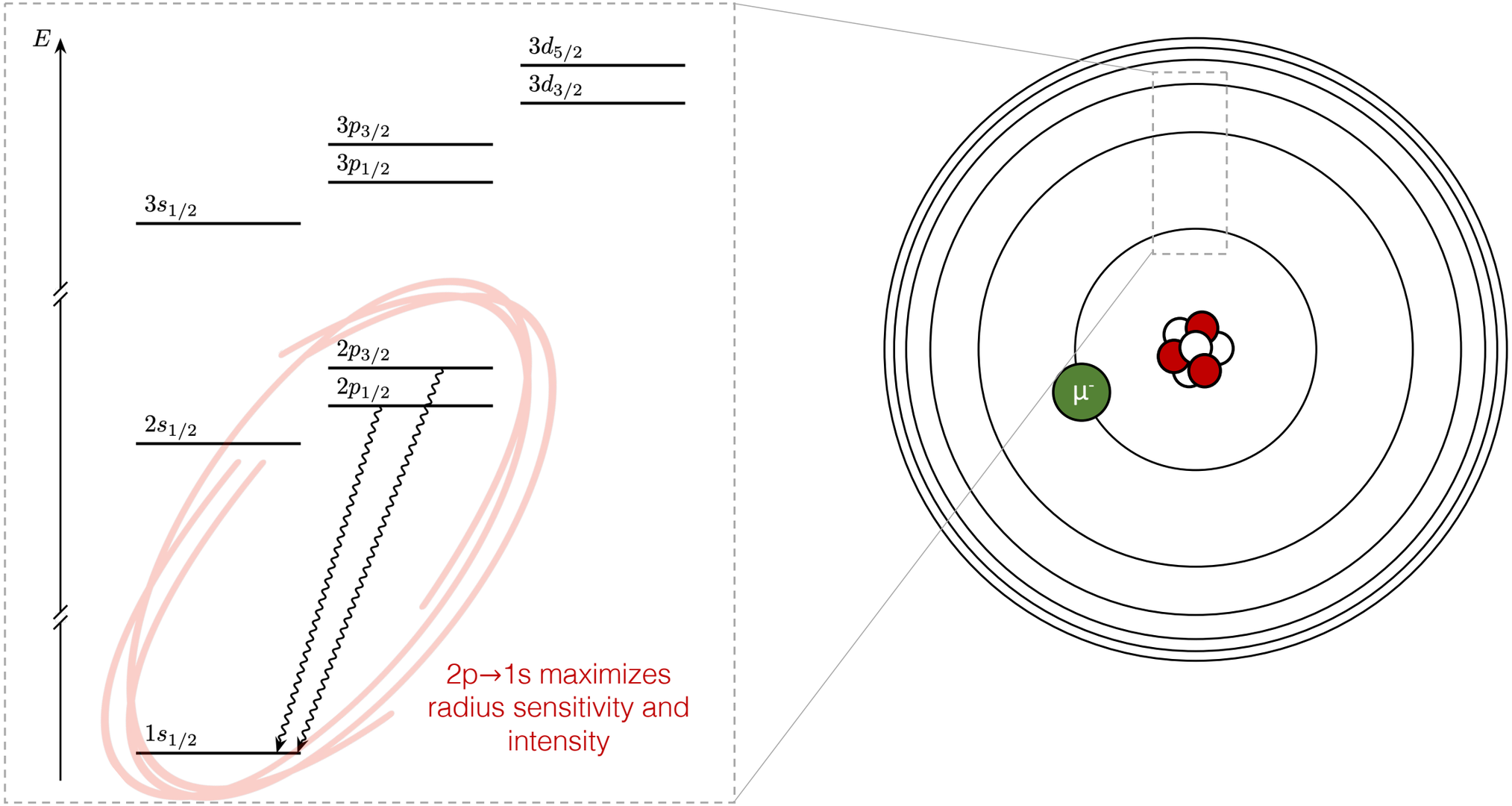

Nuclear charge radii

Why and how to measure them

Absolute nuclear charge radii

$$\langle r_c^2 \rangle = \frac{1}{Ze} \int \rho(r)\, r^2\, d\tau$$

Input for precision atomic theory

Benchmarking ab-initio nuclear theory

Nuclear structure physics

Ab-initio methods keep progressing across the nuclear chart:

DOI: 10.3389/fphy.2020.00379 (2020)

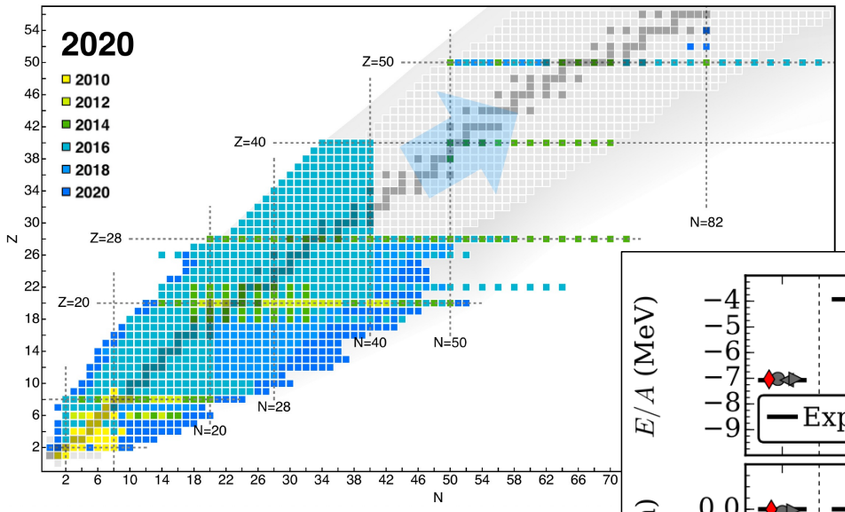

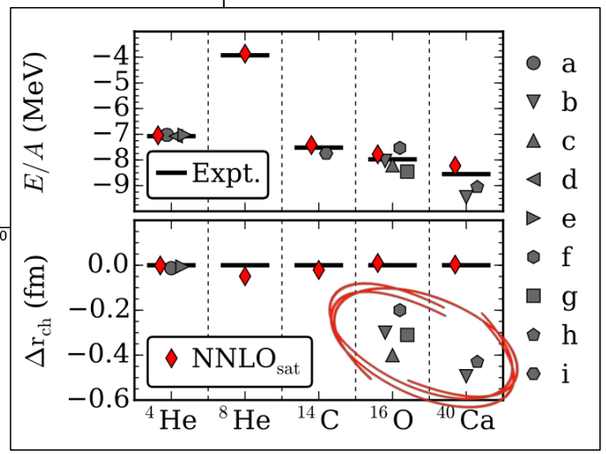

Two complementary benchmarks: energies & charge radii

DOI: 10.1103/PhysRevC.91.051301 (2015)

E.g. study of halo-nuclei:

^{11}Li

DOI: 10.1103/PhysRevC.84.024307 (2011)

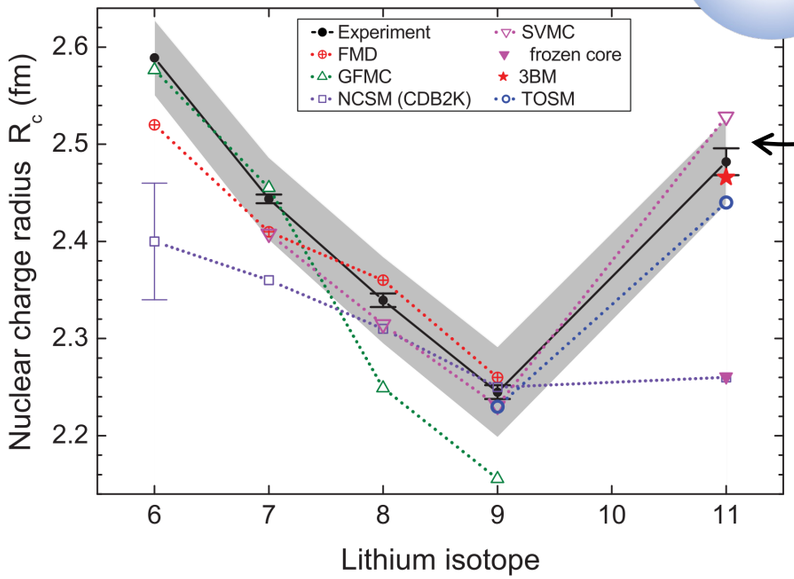

Measuring nuclear charge radii

Spectroscopy of regular atoms

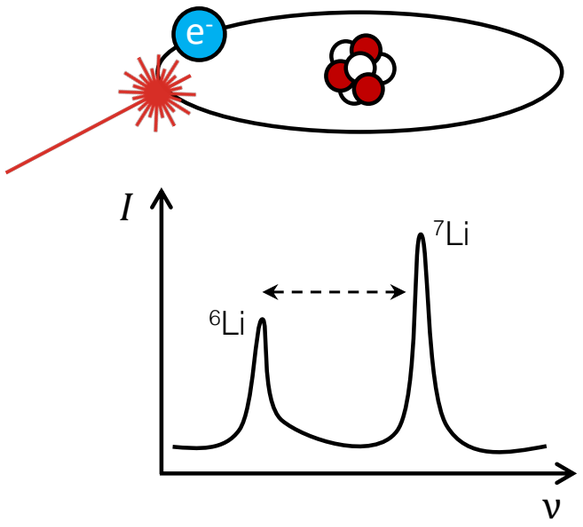

↪ Radius differences $\delta\langle r_c^2 \rangle$

Elastic electron scattering

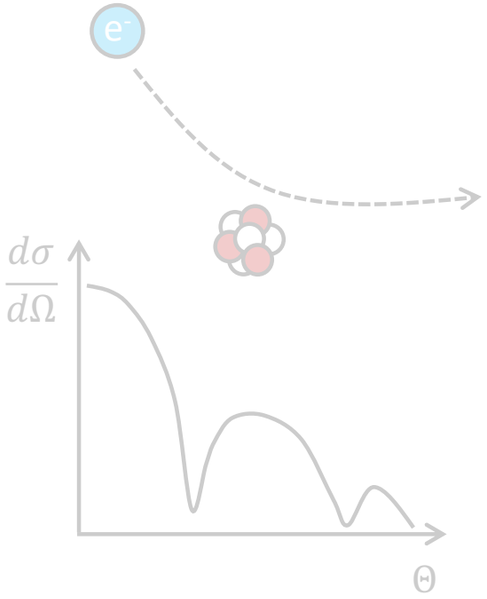

↪ Shape of the nuclear charge density distribution $\rho(r)$

Spectroscopy of muonic atoms

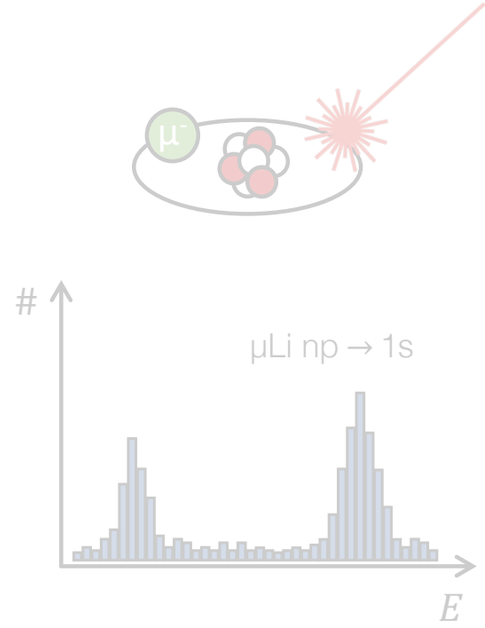

↪ Absolute nuclear charge radii $\langle r_c^2 \rangle$

Measuring nuclear charge radii

Spectroscopy of regular atoms

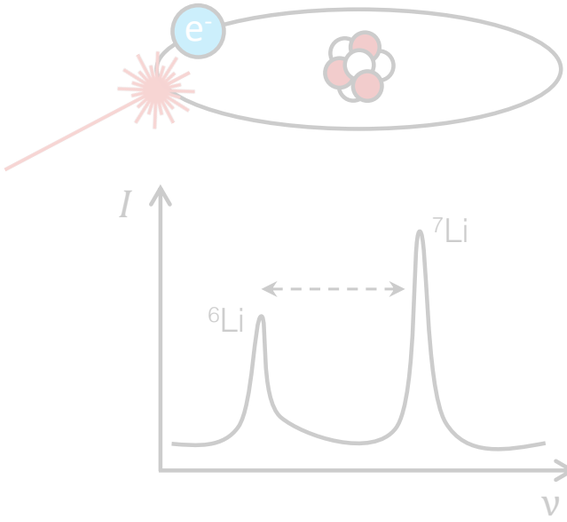

↪ Radius differences $\delta\langle r_c^2 \rangle$

Elastic electron scattering

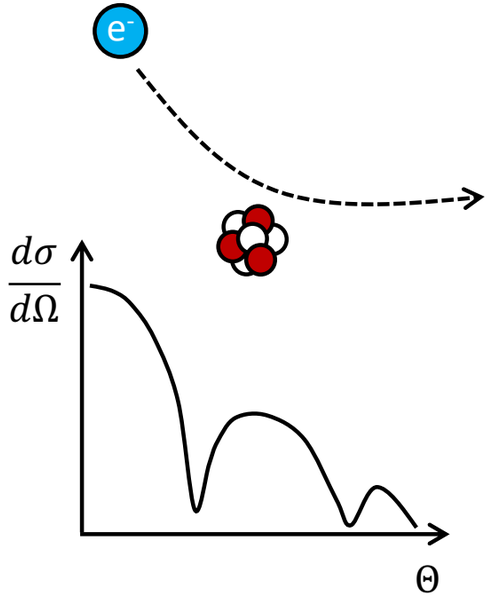

↪ Shape of the nuclear charge density distribution $\rho(r)$

Spectroscopy of muonic atoms

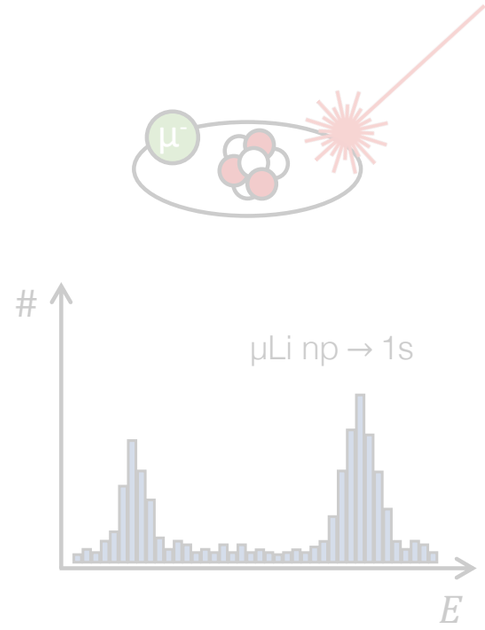

↪ Absolute nuclear charge radii $\langle r_c^2 \rangle$

Measuring nuclear charge radii

Spectroscopy of regular atoms

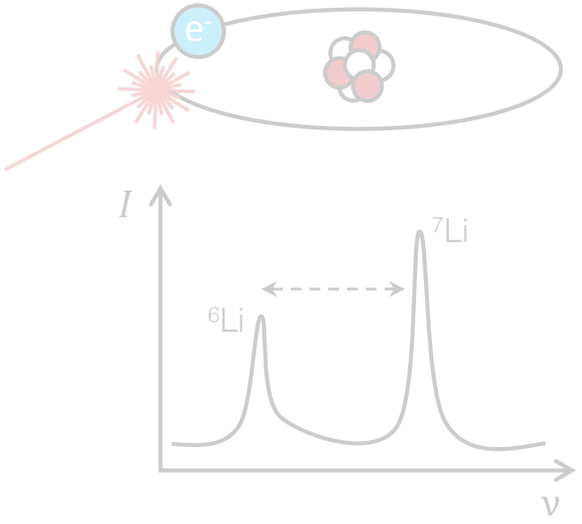

↪ Radius differences $\delta\langle r^2 \rangle$

Elastic electron scattering

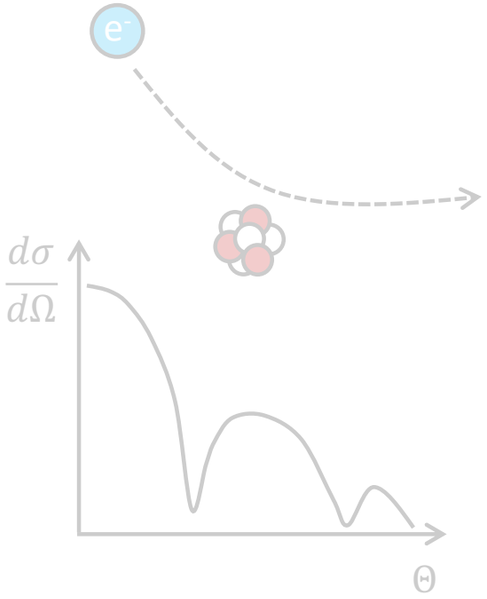

↪ Shape of the nuclear charge density distribution $\rho(r)$

Spectroscopy of muonic atoms

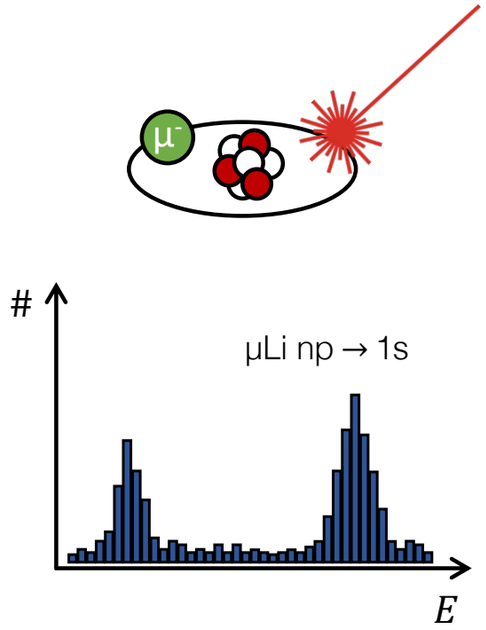

↪ Absolute nuclear charge radii $\langle r_c^2 \rangle$

Lithium nuclear charge radii

From electron scattering and isotope shift measurements

DOI: 10.1103/PhysRevC.84.024307 (2011)

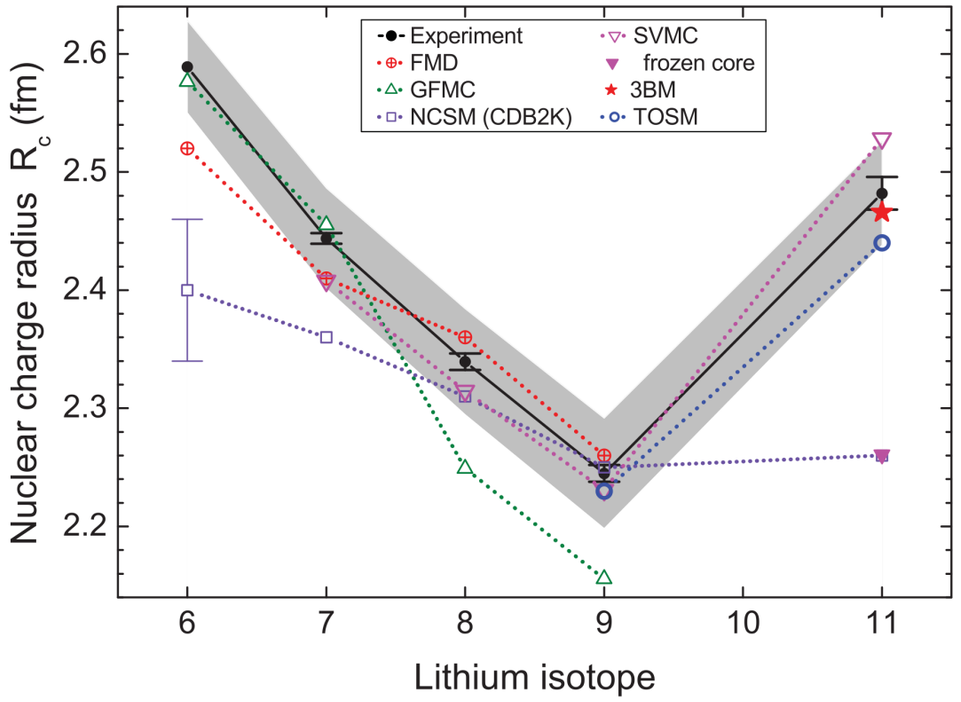

- Current literature values extracted from two inputs:
  1. Electron scattering for absolute radius reference at ^{6}Li (grey unc. band)
  2. Isotope shifts (black uncertainties) connecting within the chain up to ^{11}Li
- Whole isotopic chain currently limited by ^{6}Li anchor radius:

$$R_c(^{6}\mathrm{Li}) = 2.589(39)\ \mathrm{fm}$$

Theory community still actively updating, e.g.:

- X.-X. Sun, H. Le, U.-G. Meißner, and A. Nogga, “Radii of light nuclei from the Jacobi no-core shell model“, *Phys. Rev. C* 112, 024317 (**2025**).
- M. Knöll, M. Lockner, P. Maris, R. J. McCarty, R. Roth, J. P. Vary, and T. Wolfgruber, “Benchmarking ANN extrapolations of the ground-state energies and radii of Li isotopes”, arXiv:2501.18252 (**2025**).

Muonic Lithium

2p-1s multiplet level scheme:

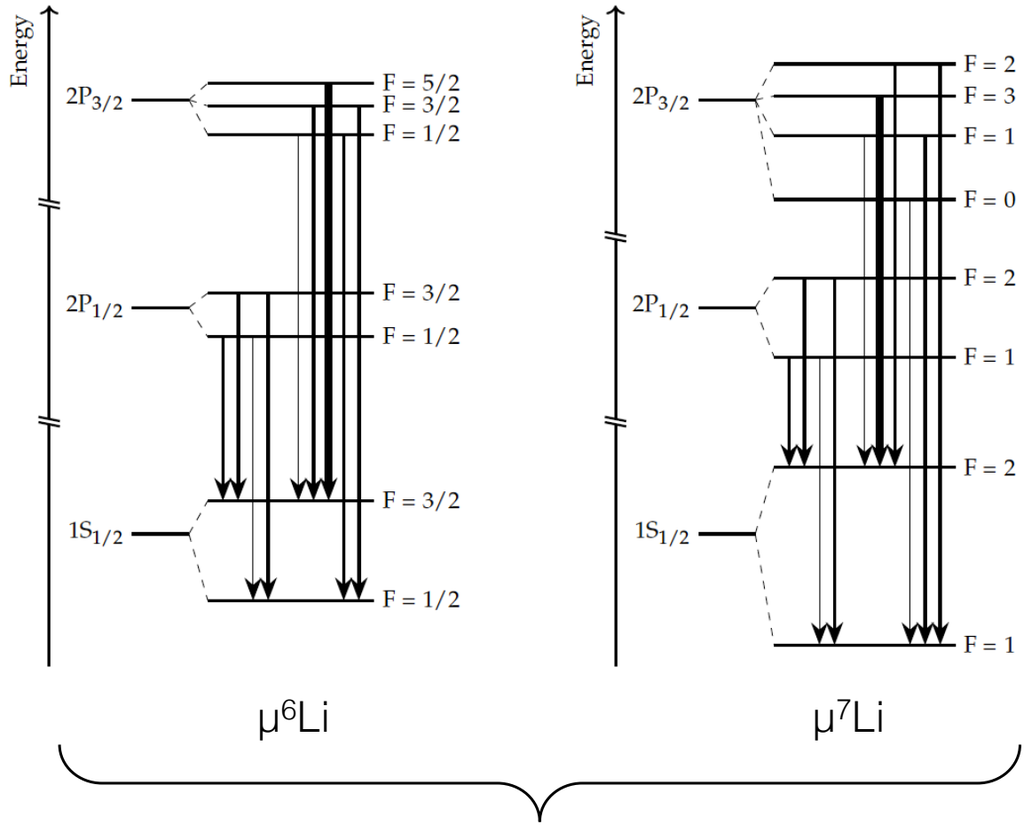

2 isotopes with hyperfine structure
= 19 lines within less than 60 eV!

Muonic Lithium

2p-1s multiplet level scheme:

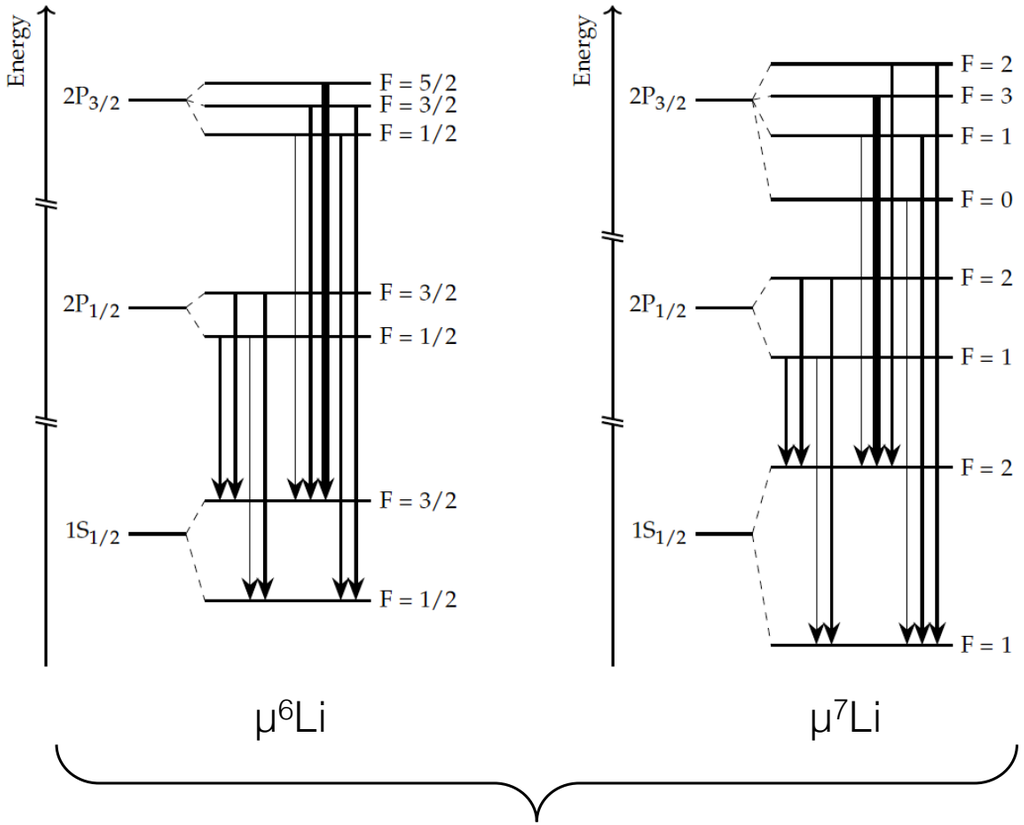

2 isotopes with hyperfine structure
= 19 lines within less than 60 eV!

Expected spectrum with conventional detector:

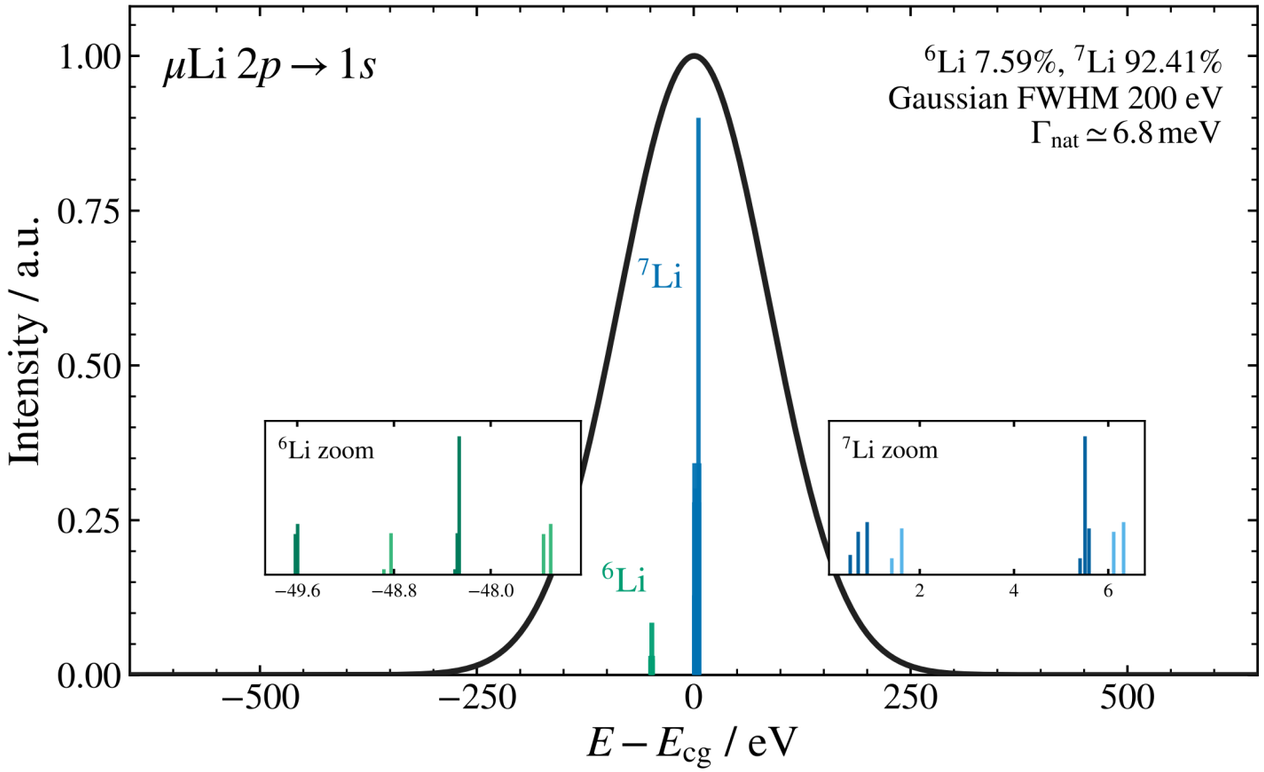

Typical resolution of semiconductor detectors:
> 200 eV @ 18 keV

“Latest” muonic lithium spectroscopy result

VOLUME 20, NUMBER 10 PHYSICAL REVIEW LETTERS 4 MARCH 1968

ENERGY AND WIDTH MEASUREMENTS OF LOW-Z PIONIC X-RAY TRANSITIONS*

R. J. Harris, Jr.,† W. B. Shuler, M. Eckhause, R. T. Siegel, and R. E. Welsh
College of William and Mary, Williamsburg, Virginia
(Received 15 January 1968)

Element	E_{exp}		Radius (fm) - Equivalent Uniform Charge	
	This Work	Other	This Work	Electron Scattering
Li^6	18.64±0.07	18.1 ±0.4 [b]	4.96±6.0	3.28±0.06 [e]
Li^7	18.69±0.06	18.1 ±0.4 [b]	4.94±5.0	3.09±0.04 [e]

Radius uncertainty from 1968 measurement: >100%

⇒ Cross-check of radii by muonic atom measurement so far not possible

The “radius gap” in the low-Z range

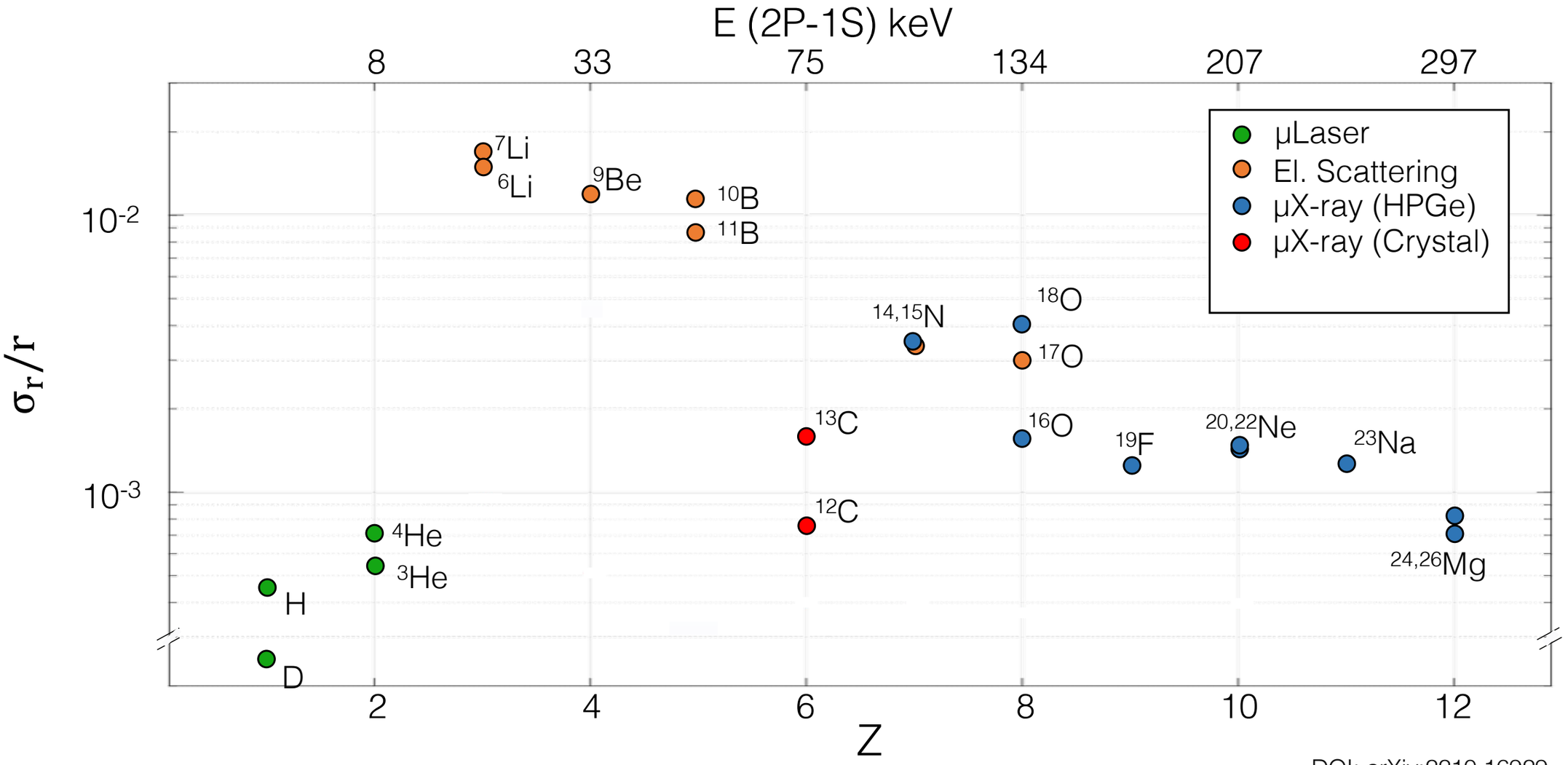

DOI: arXiv:2210.16929

The “radius gap” in the low-Z range

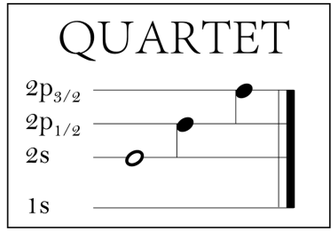

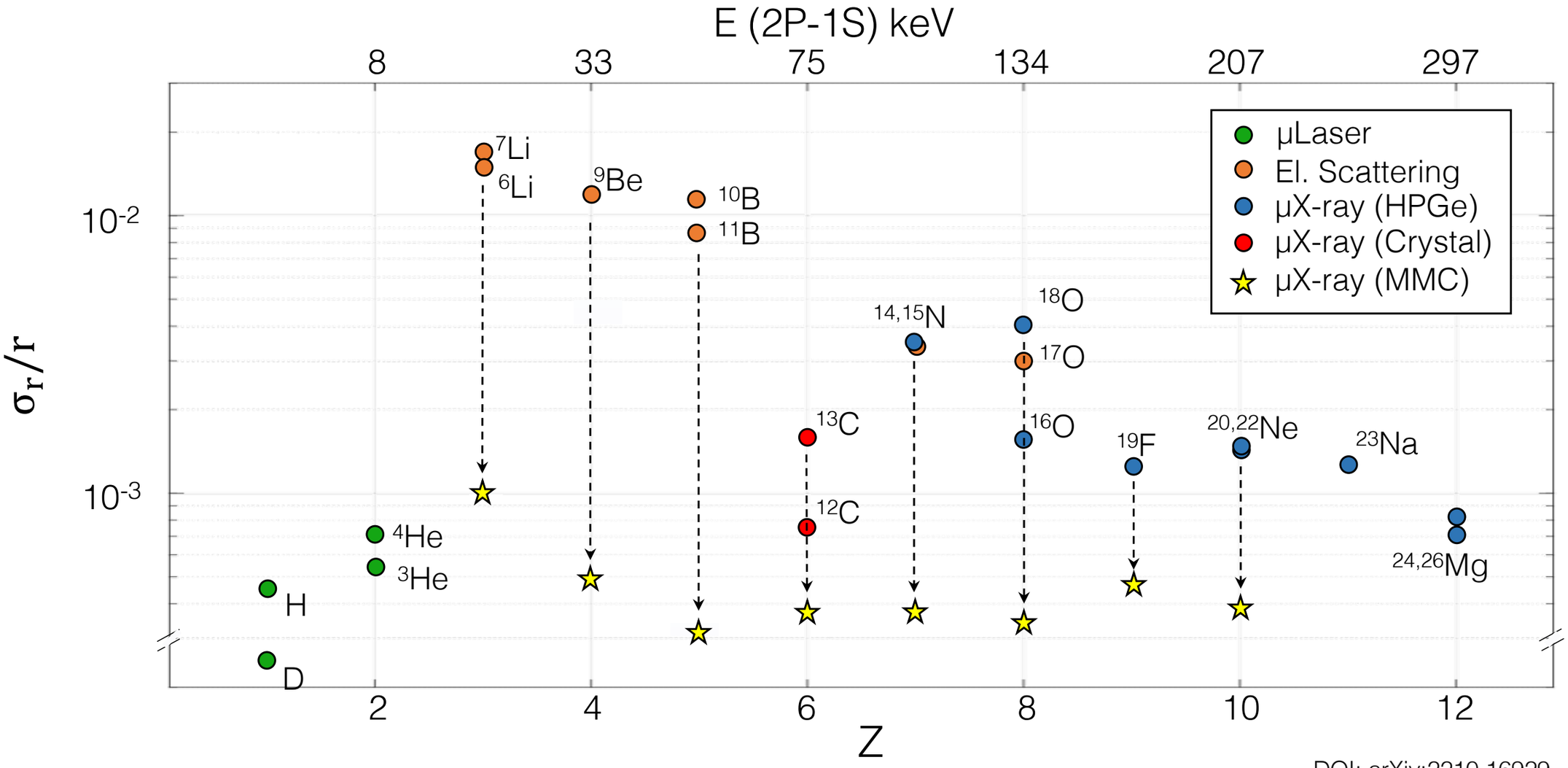

DOI: arXiv:2210.16929

Experimental approach

using metallic magnetic calorimeters

Metallic magnetic calorimeters (MMC)

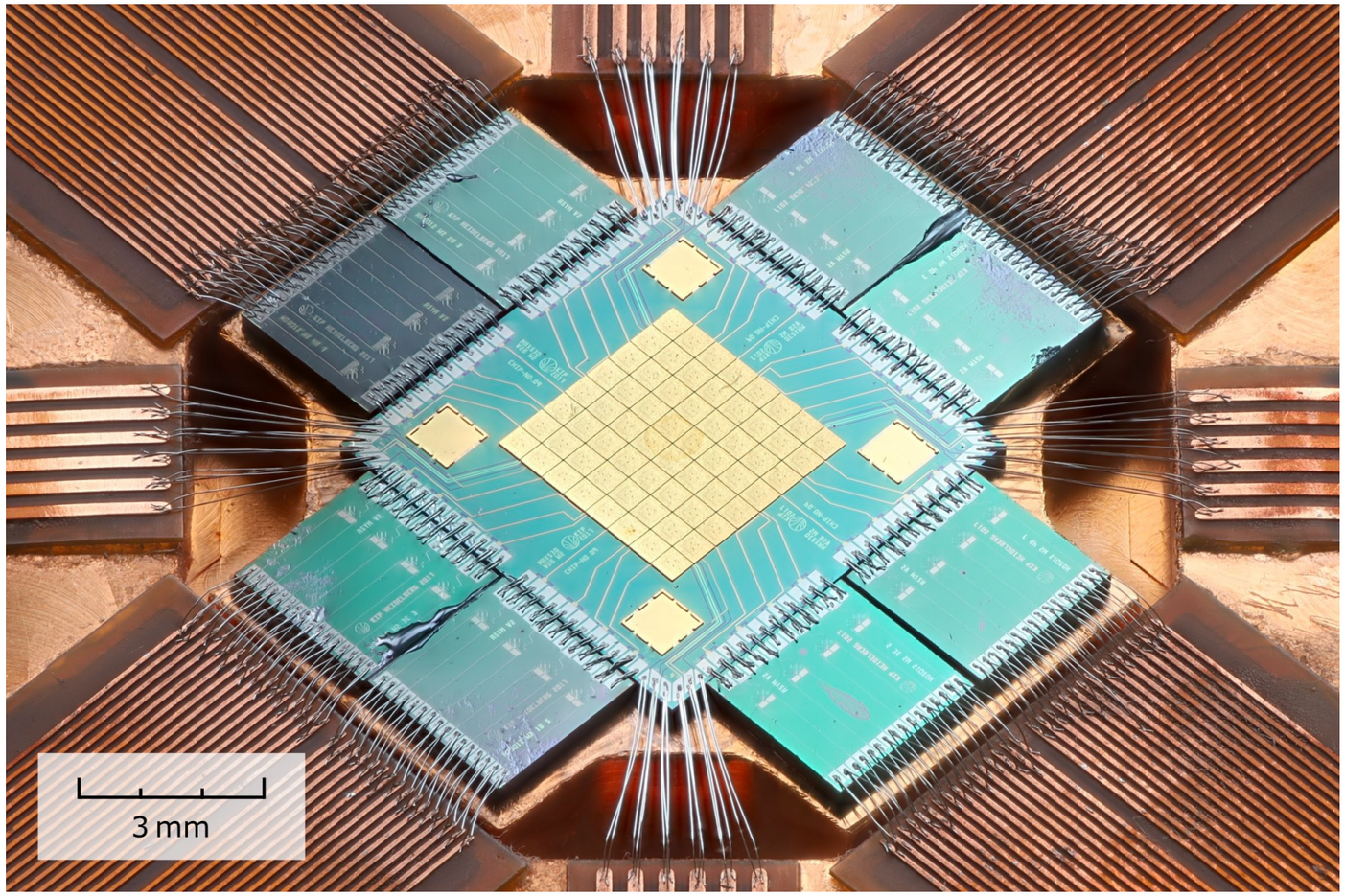

DOI: 10.1007/s10909-024-03141-x

- Cryogenic detector at 10 – 20 mK
- 64 absorbers, each 500 µm x 500 µm x 20 µm

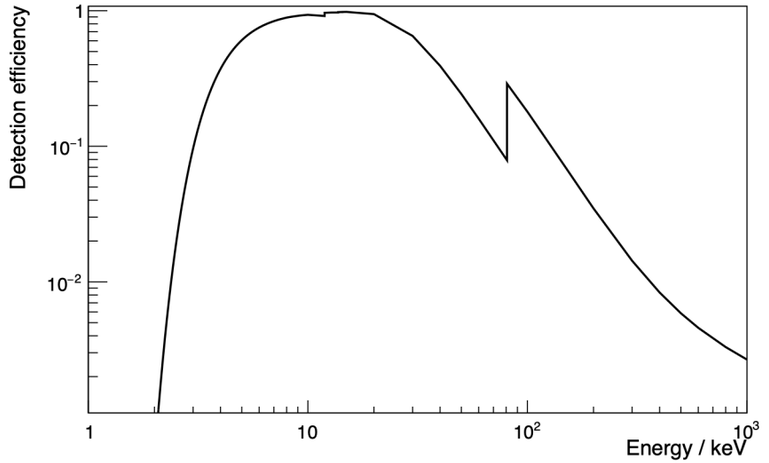

Combining:

- High efficiency: > 90% from 8 – 22 keV
- High resolution: ~10 – 20 eV at 18 keV

→ 10 – 20 times better
than semiconductor detectors

MMC working principle

$$\Delta T = \frac{E_\gamma}{C_{\mathrm{tot}}}$$

$$\Delta V \propto \Delta M \propto E_\gamma$$

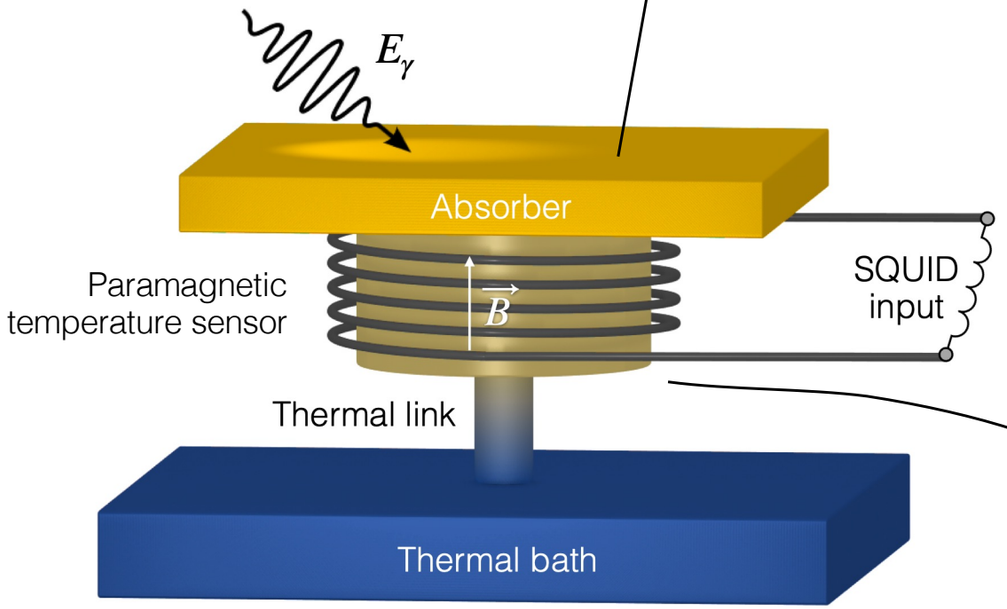

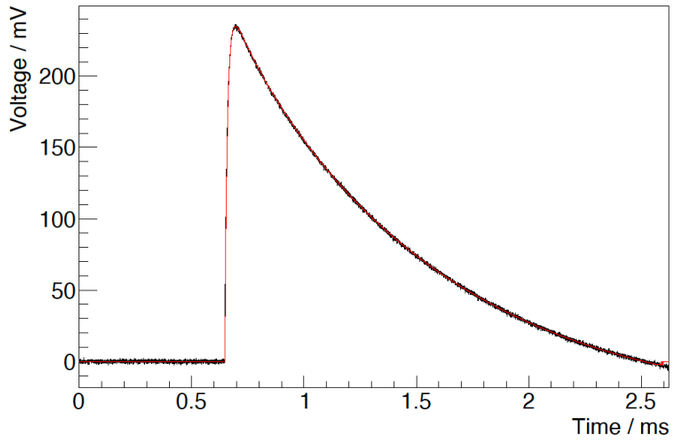

$$\Delta M = \frac{\partial M}{\partial T}\Delta T$$

MMC working principle

$\Delta V \propto \Delta M \propto E_\gamma$

$\Delta T = \frac{E_\gamma}{C_{\mathrm{tot}}}$

tunes detection efficiency → determines C_{abs}

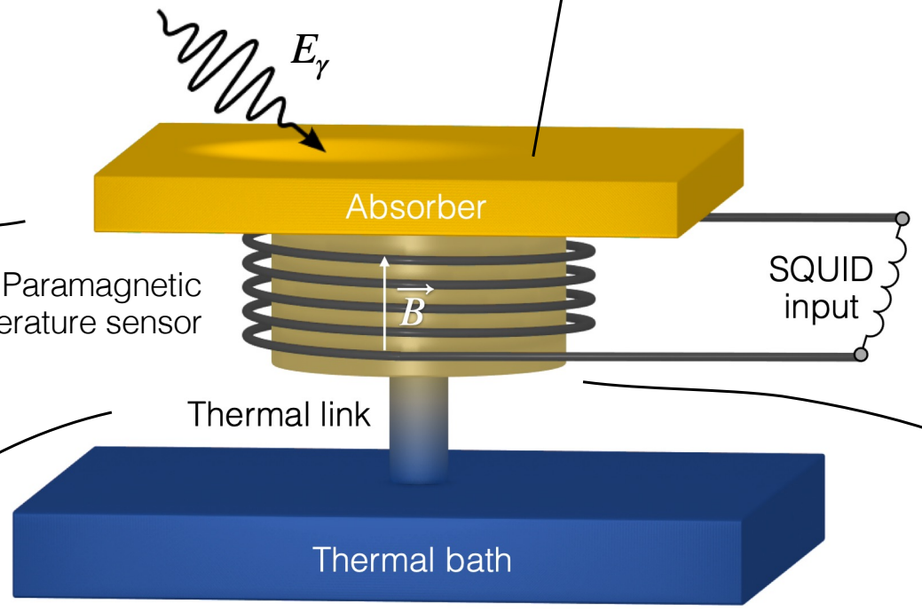

tunes signal decay time τ_D → detection speed

$\Delta M = \frac{\partial M}{\partial T}\Delta T$

Energy resolution:

$$\Delta E \propto \frac{T\sqrt{C_{abs}}}{\sqrt[4]{\tau_D}}$$

Setup October 2024

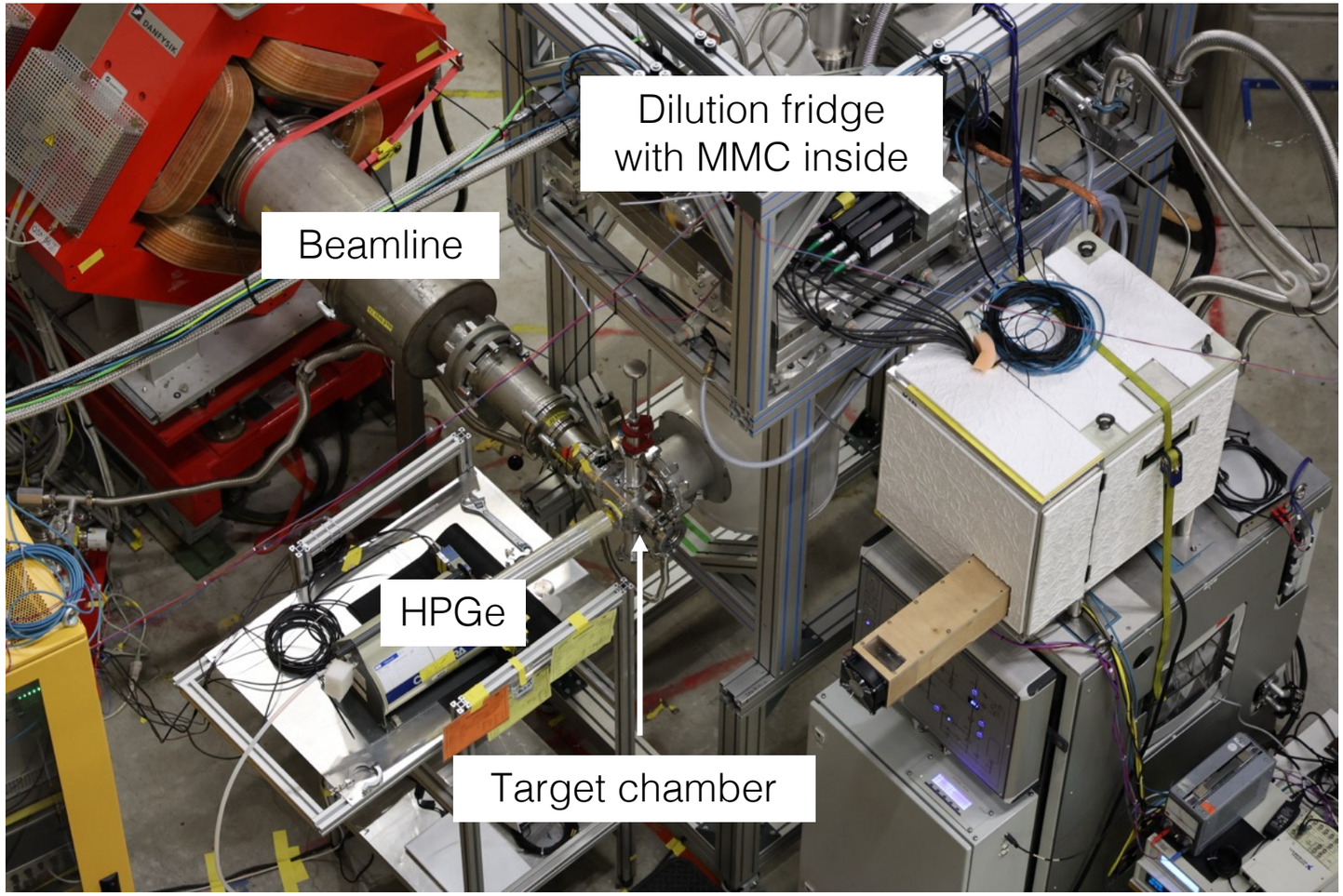

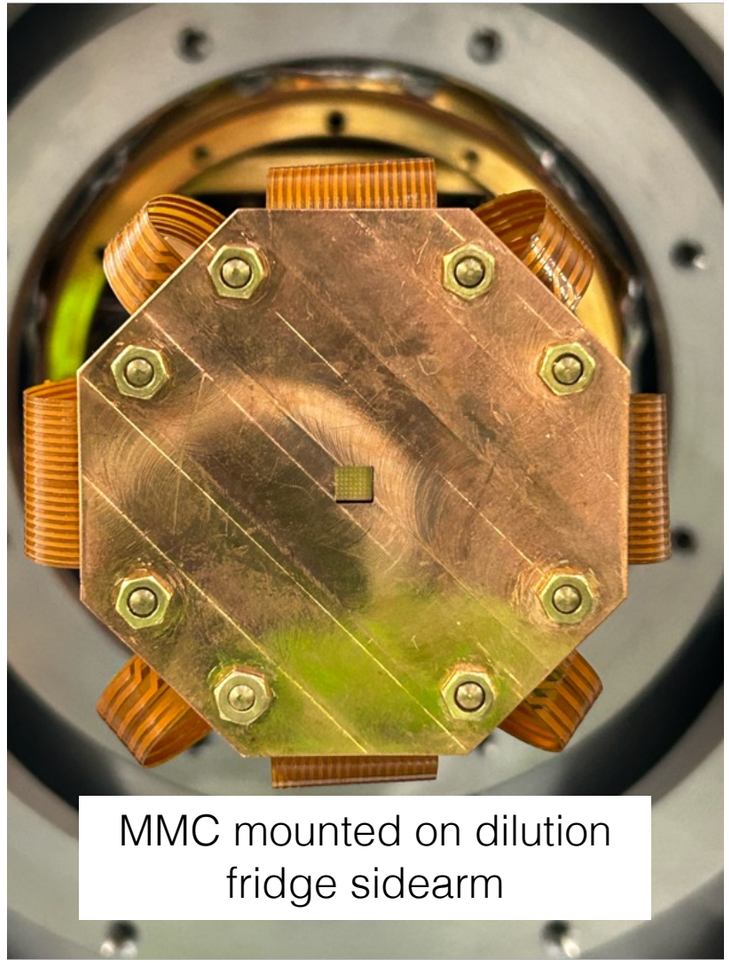

Setup October 2024

Target chamber top view

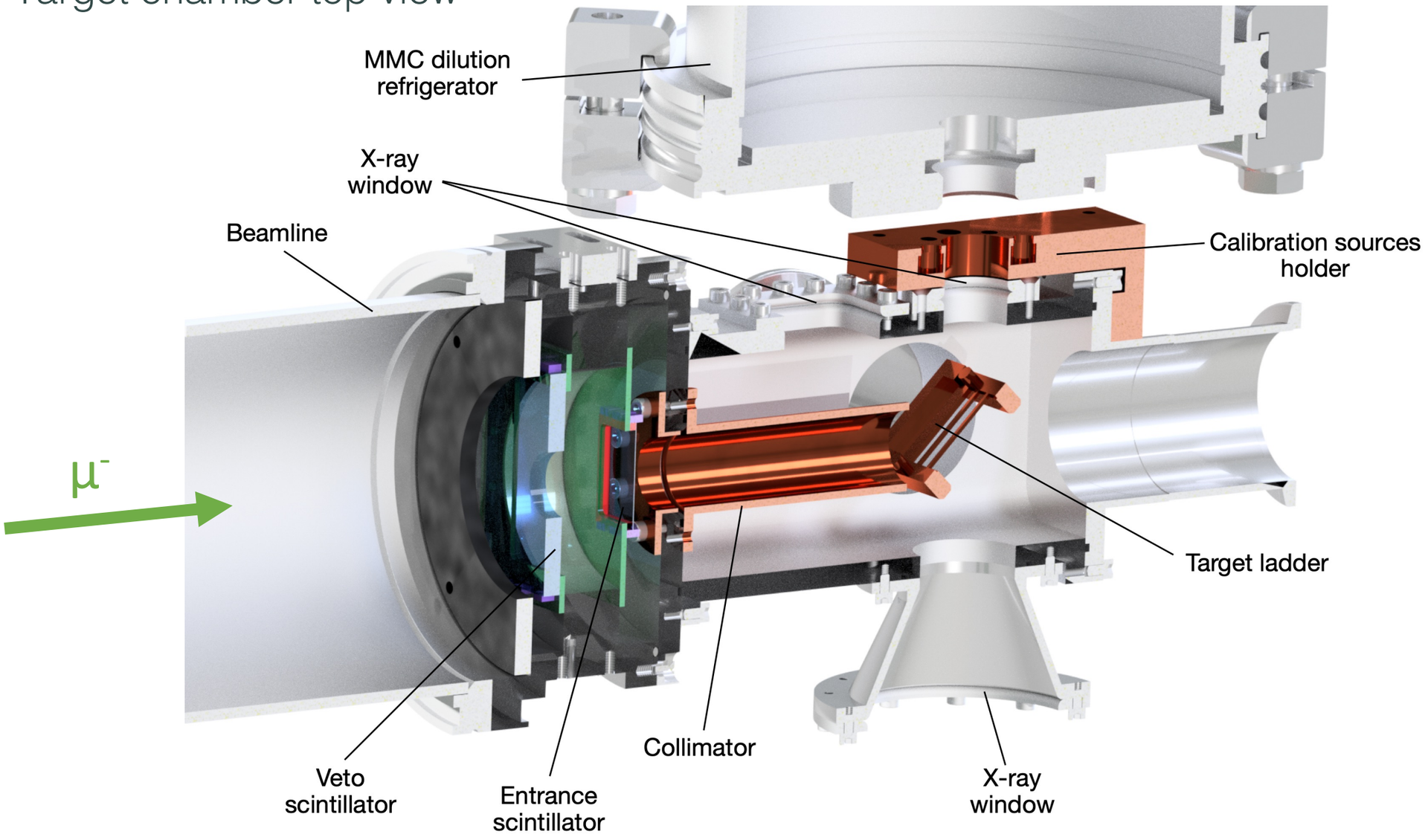

Lithium targets:

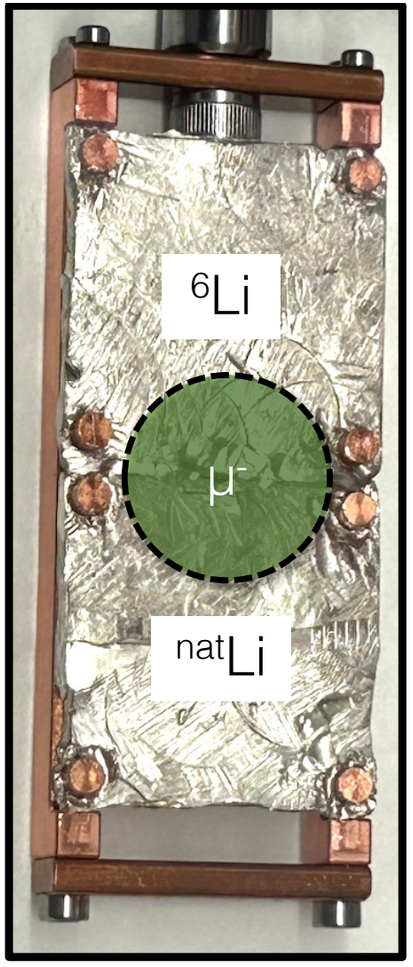

Analysis and results

Analysis pipeline

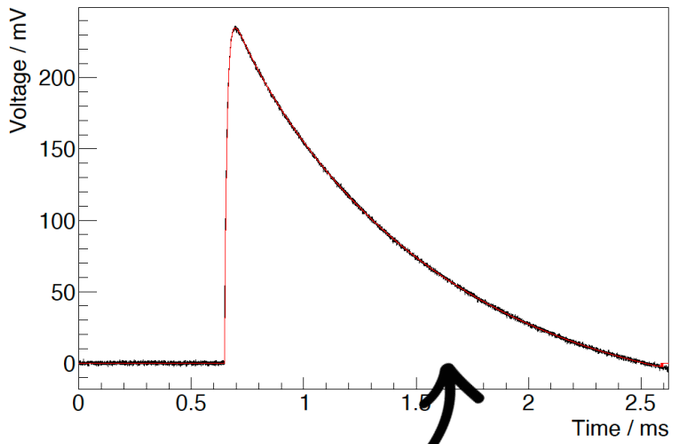

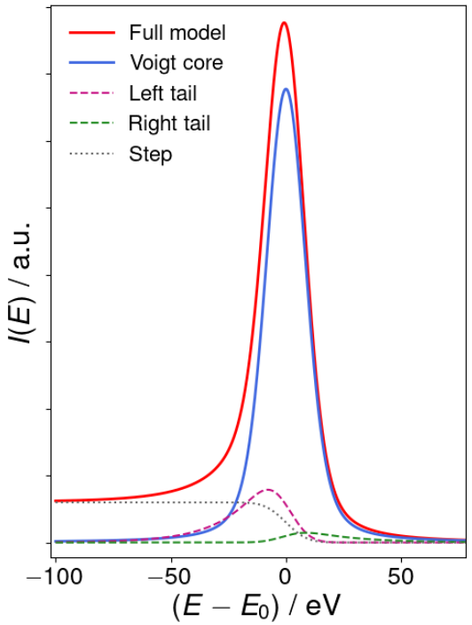

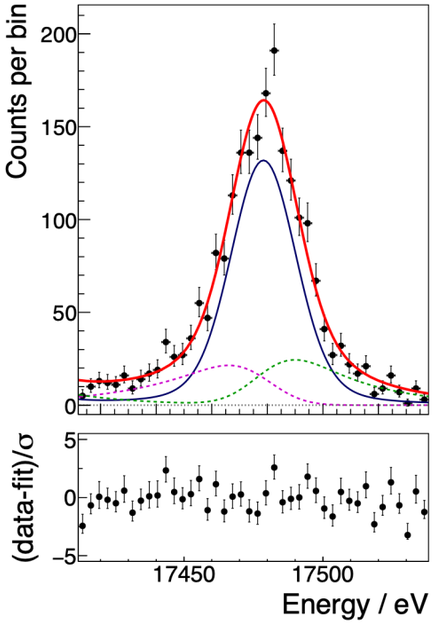

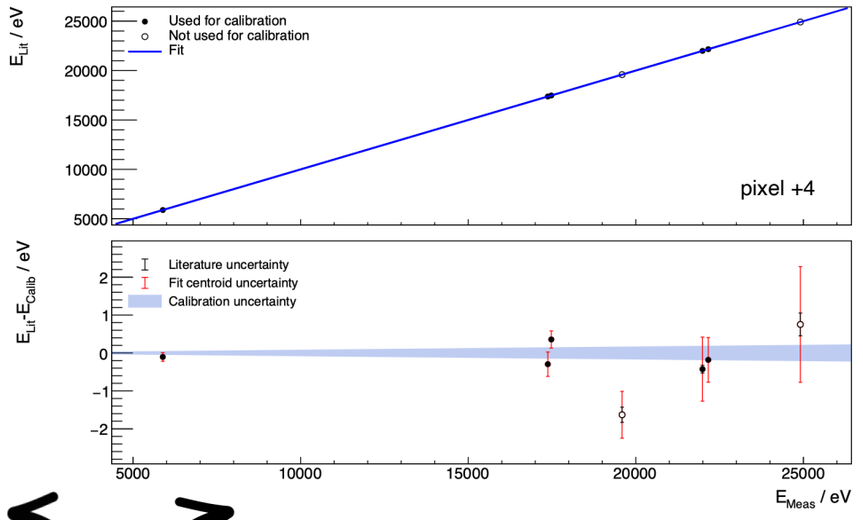

ADC calibration → fitting pulses → event identification → correct temperature & gain drifts → line shape analysis & energy calib. → energy meas.

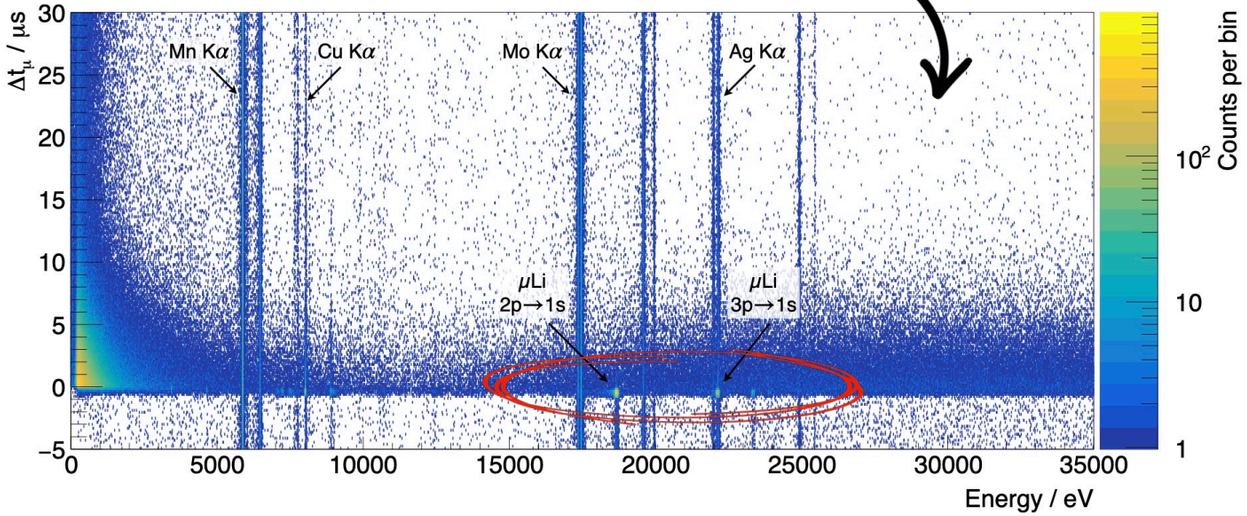

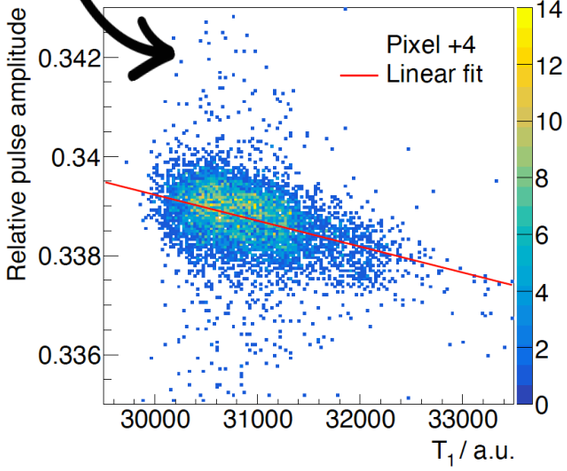

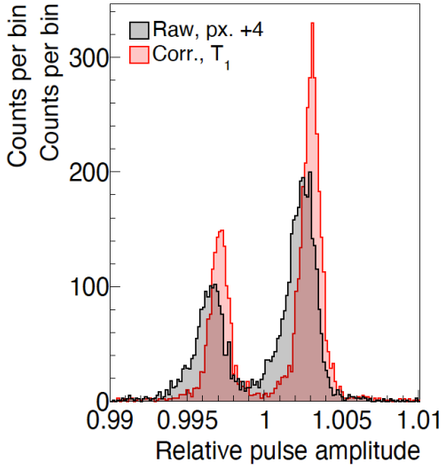

Resulting spectra

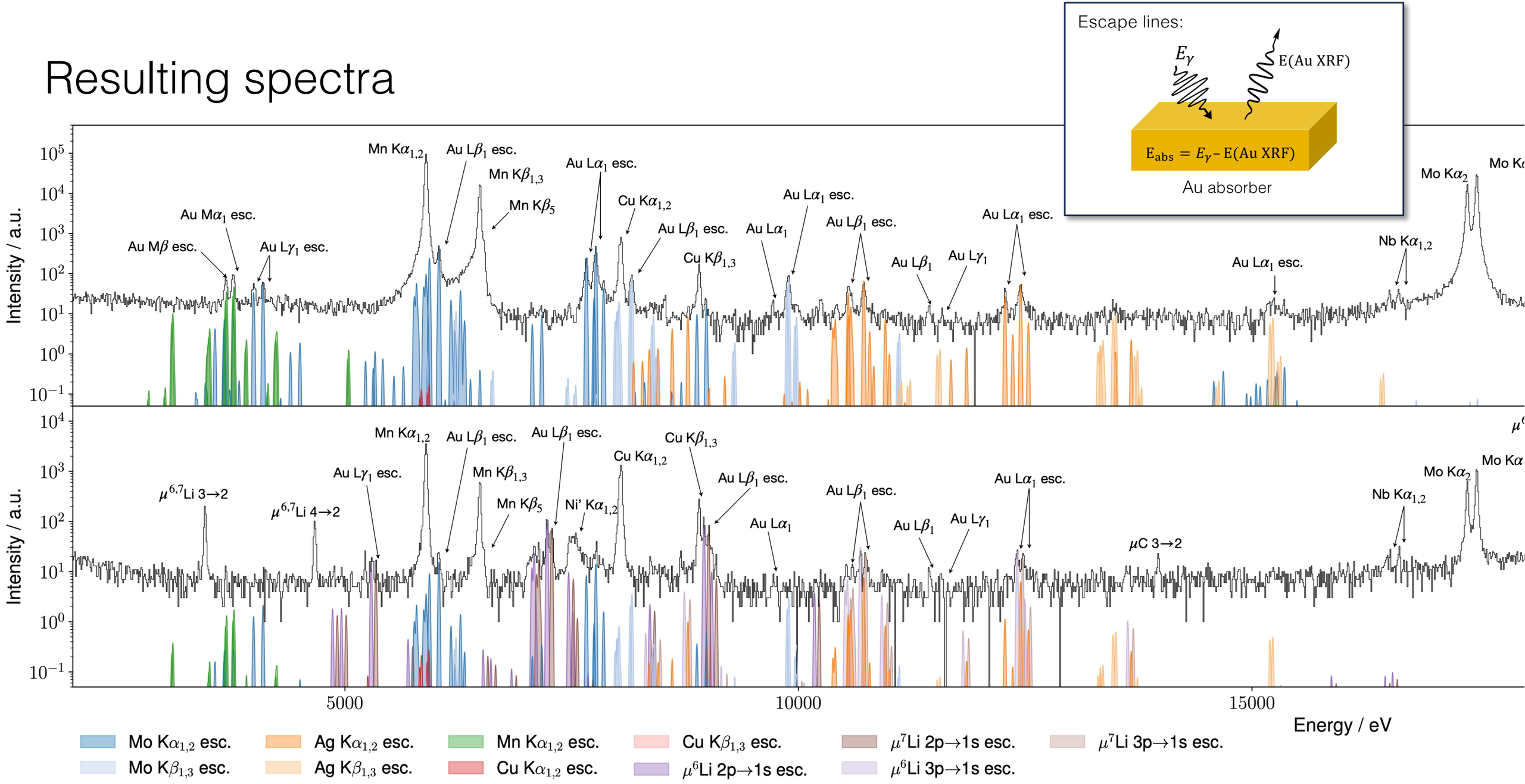

Resulting spectra

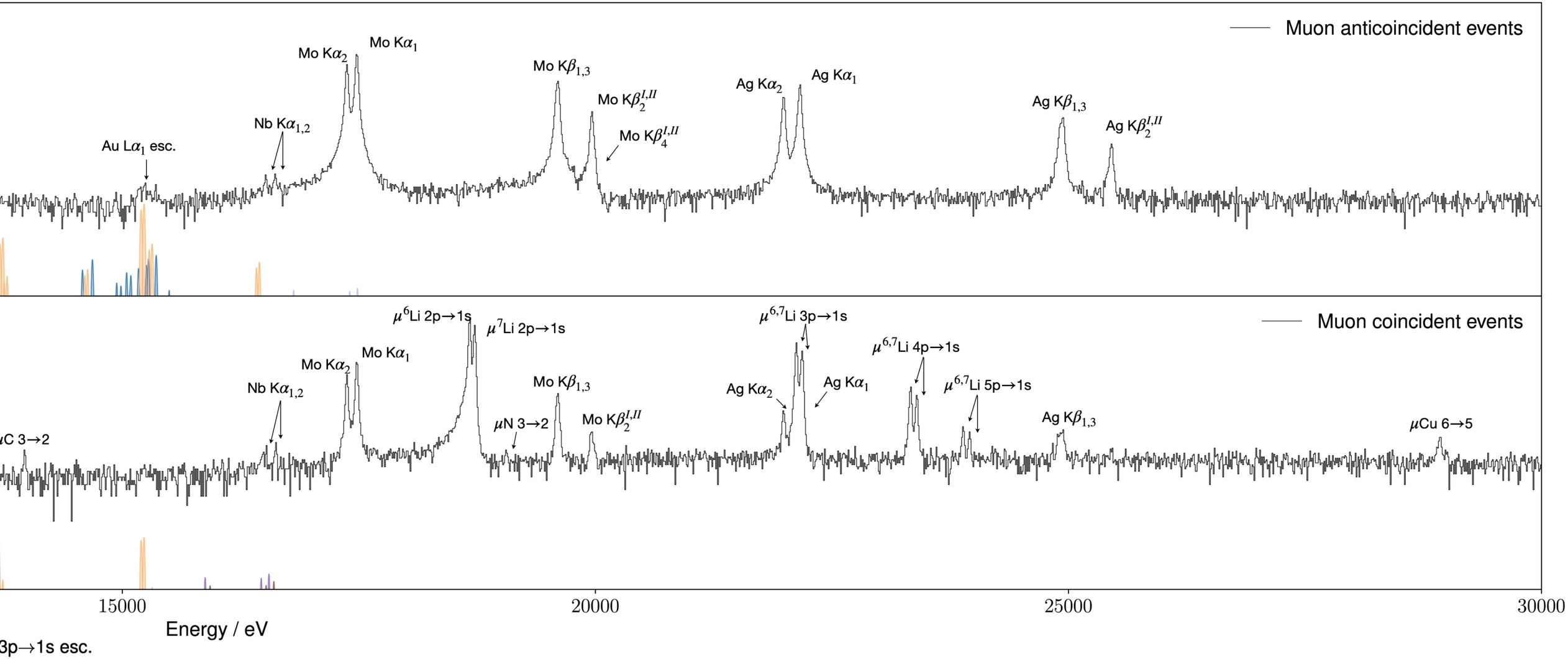

Resulting spectra

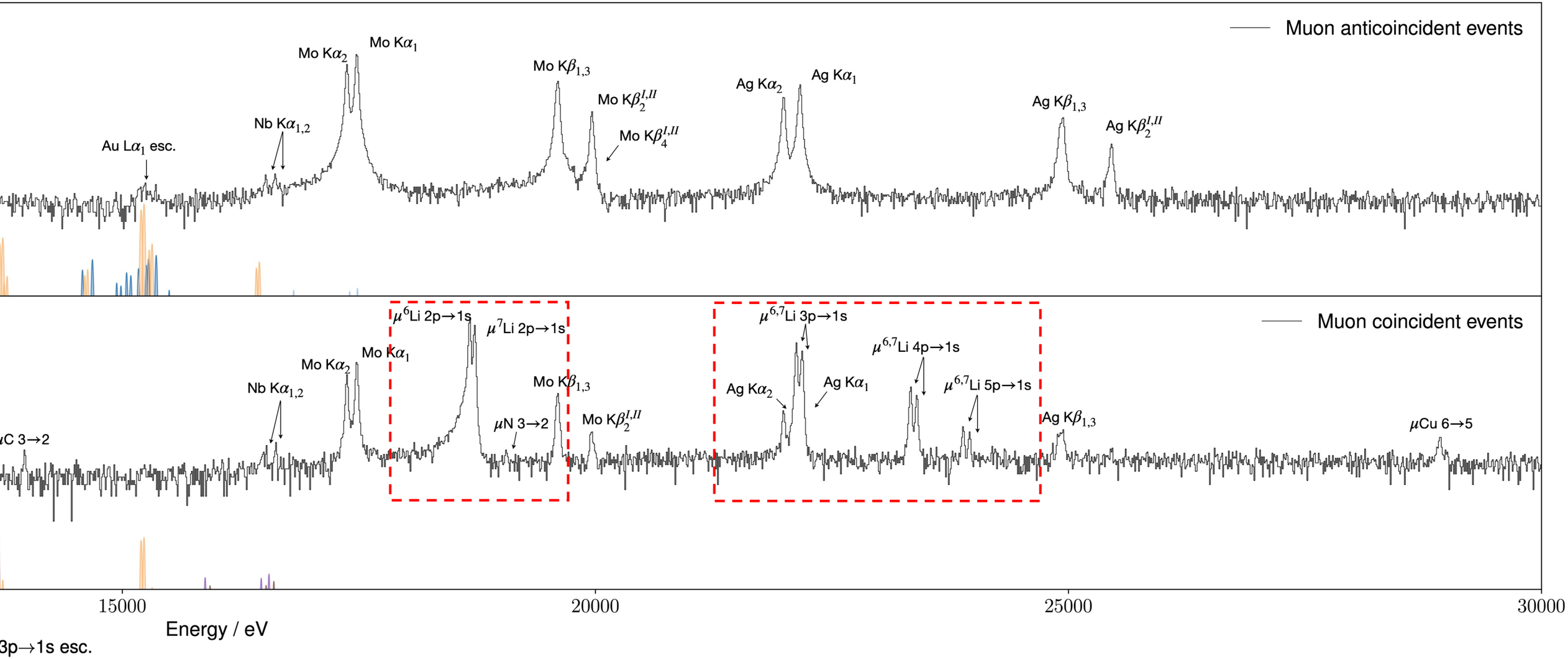

Lithium 2p–1s transition

known from calibration lines

Instrumental line shape * lithium model

theory input

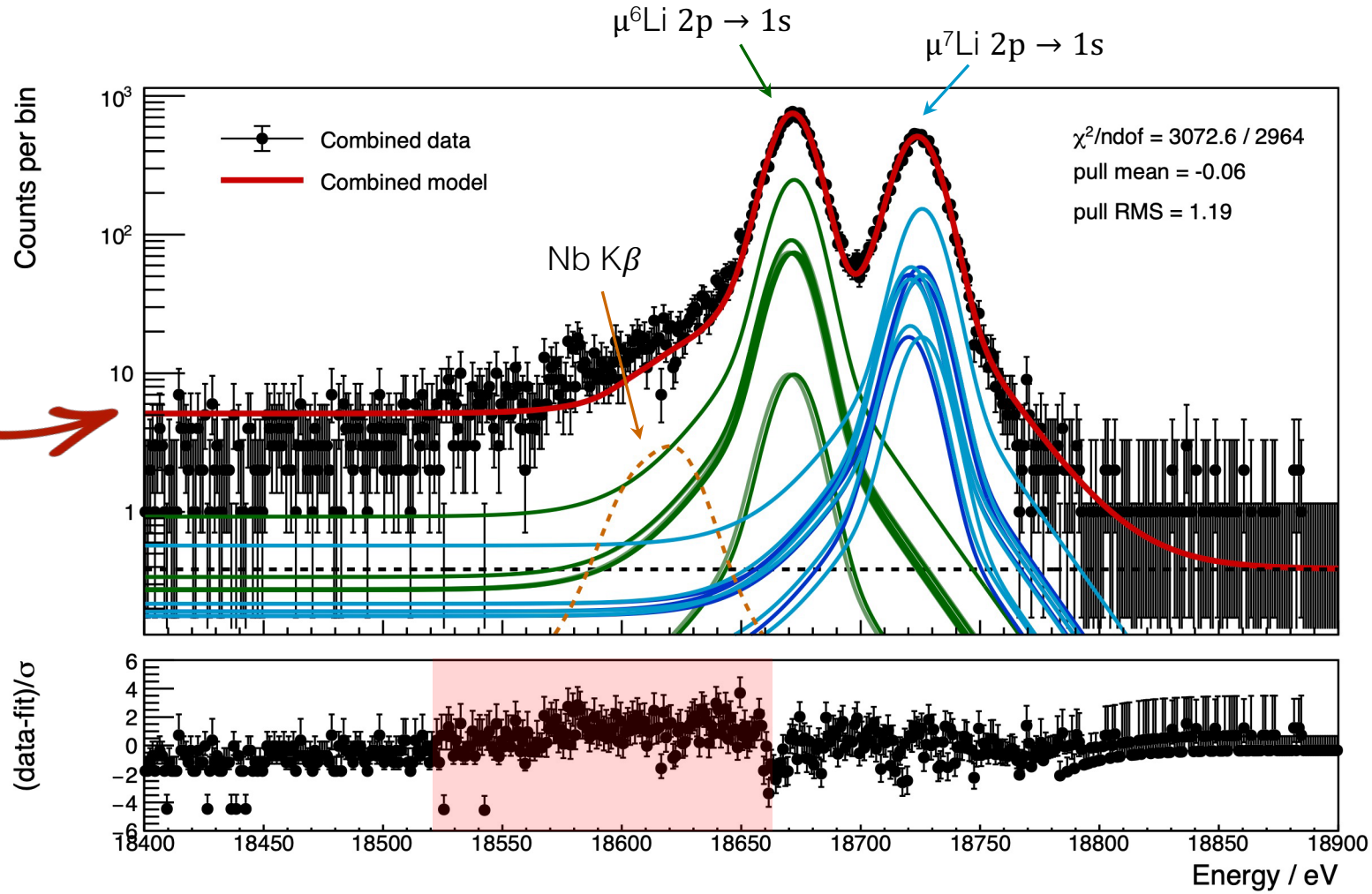

Lithium 2p–1s transition

known from calibration lines

Instrumental line shape * lithium model

theory input

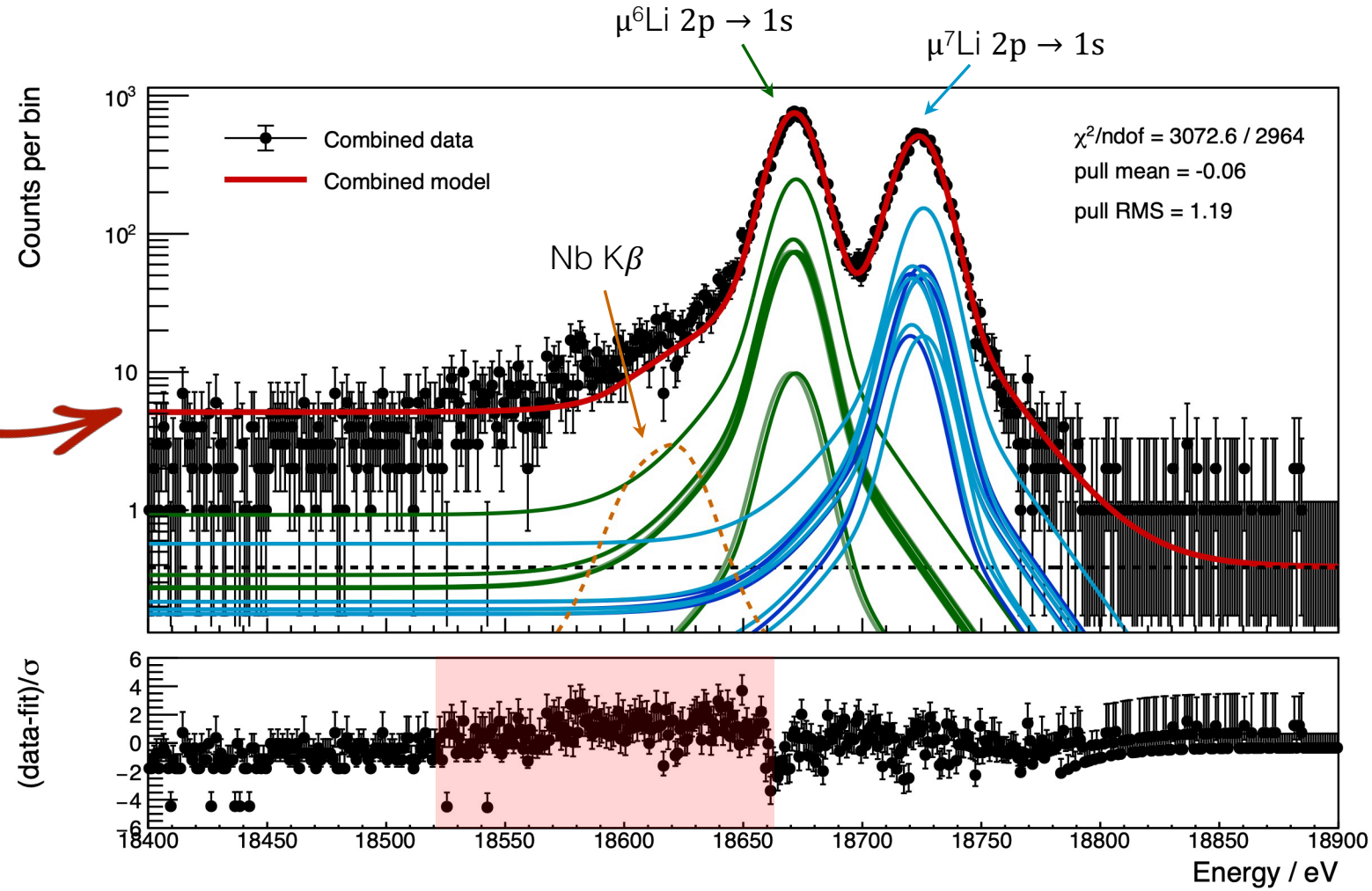

⟹ Why does the model not capture this low-energy tail?

Other lithium transitions

Higher np–1s transitions don't show this low energy excess:

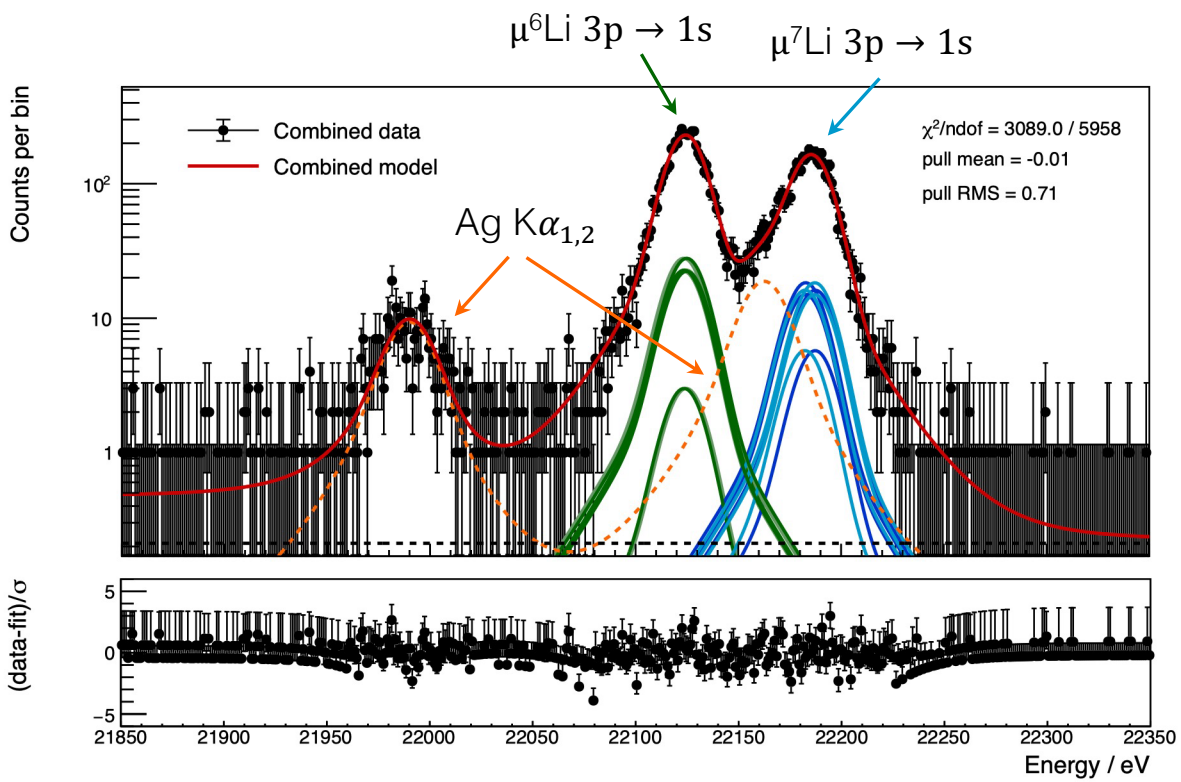

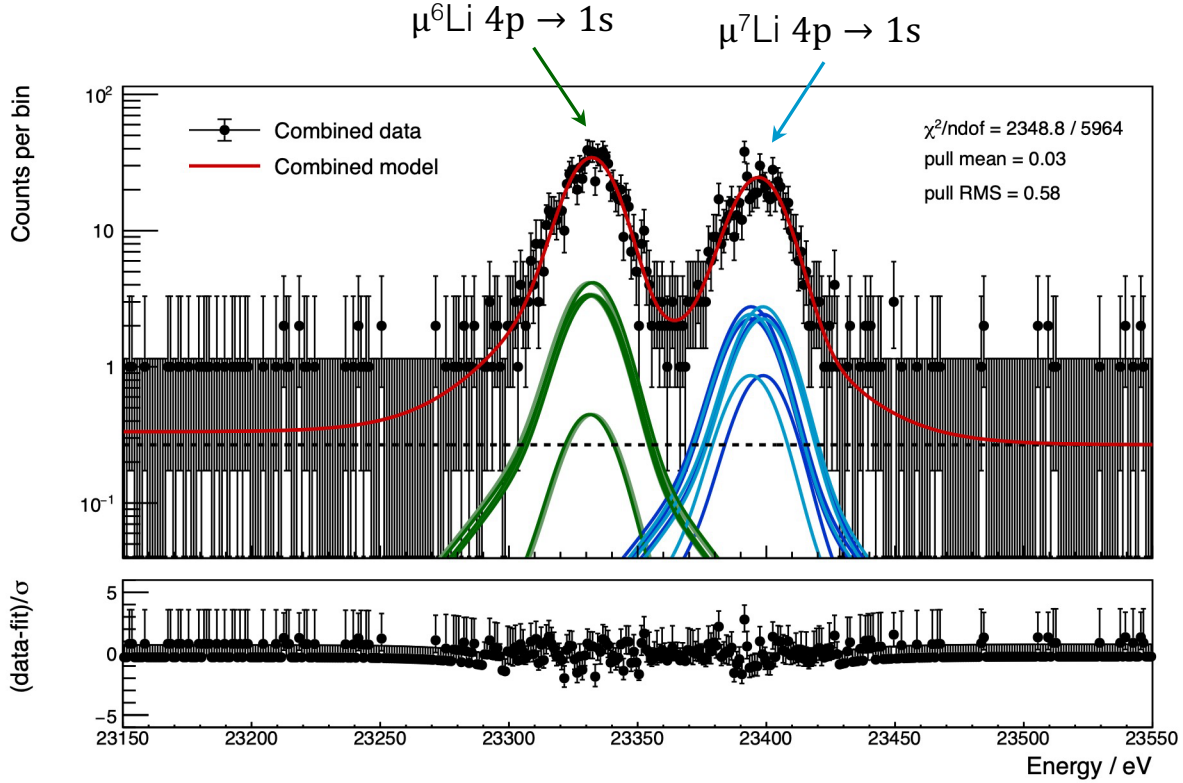

⟹ This problem is specific to the 2p–1s line of μLi!

The simplified picture of the muonic lithium atom

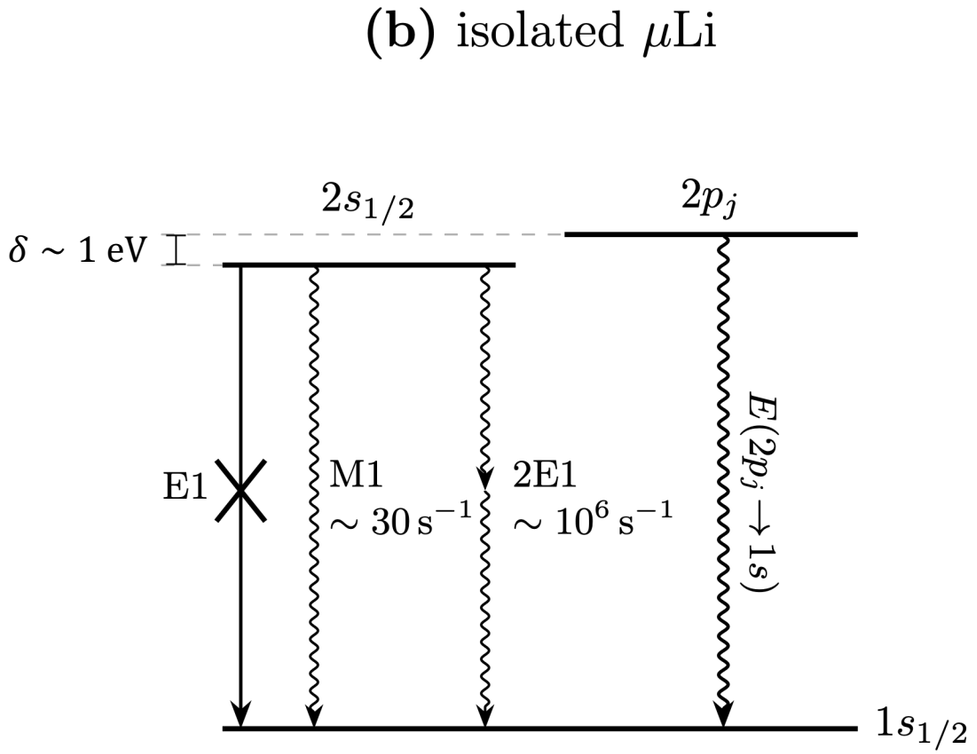

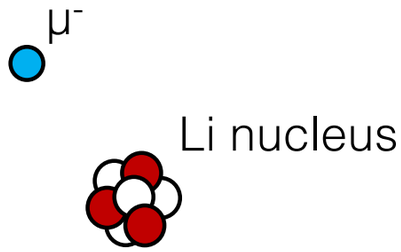

The simplified picture of the muonic lithium atom ...is too simplified

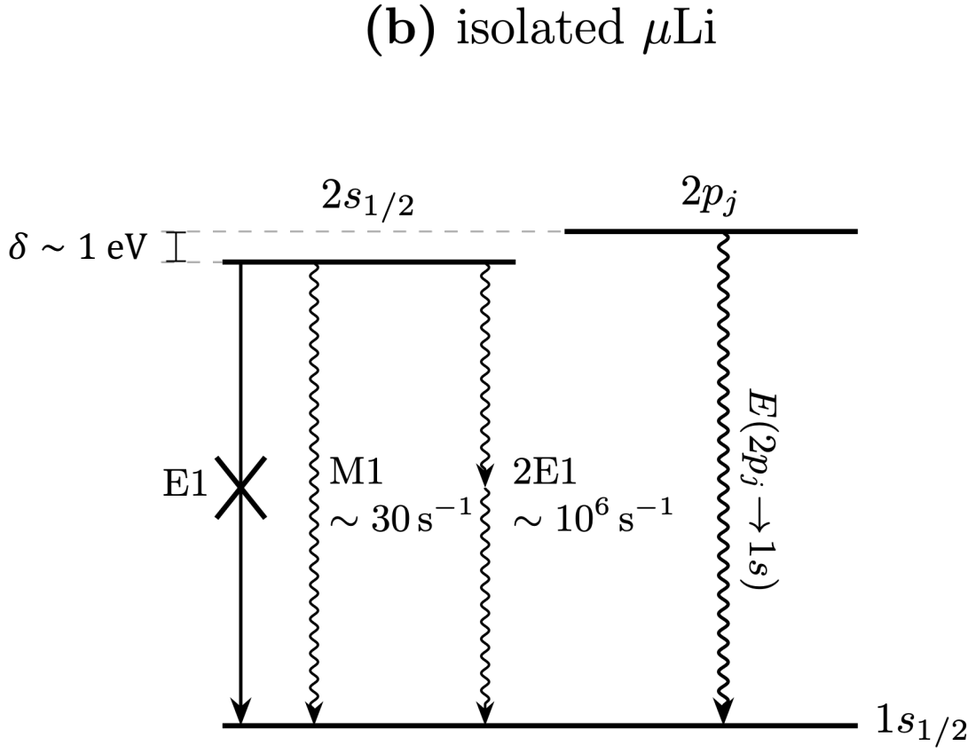

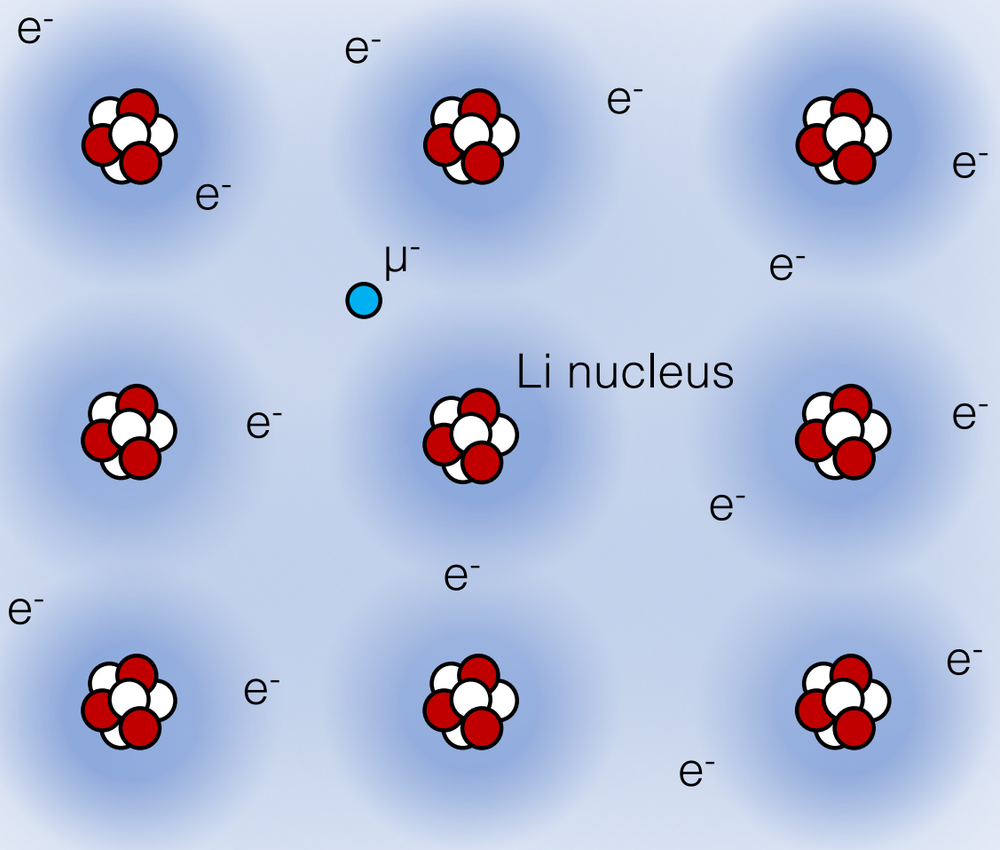

The ~~simplified~~ better picture of the muonic lithium atom

⟹ Presence of conduction electrons results in a broad, continuous 2s-1s satellite!

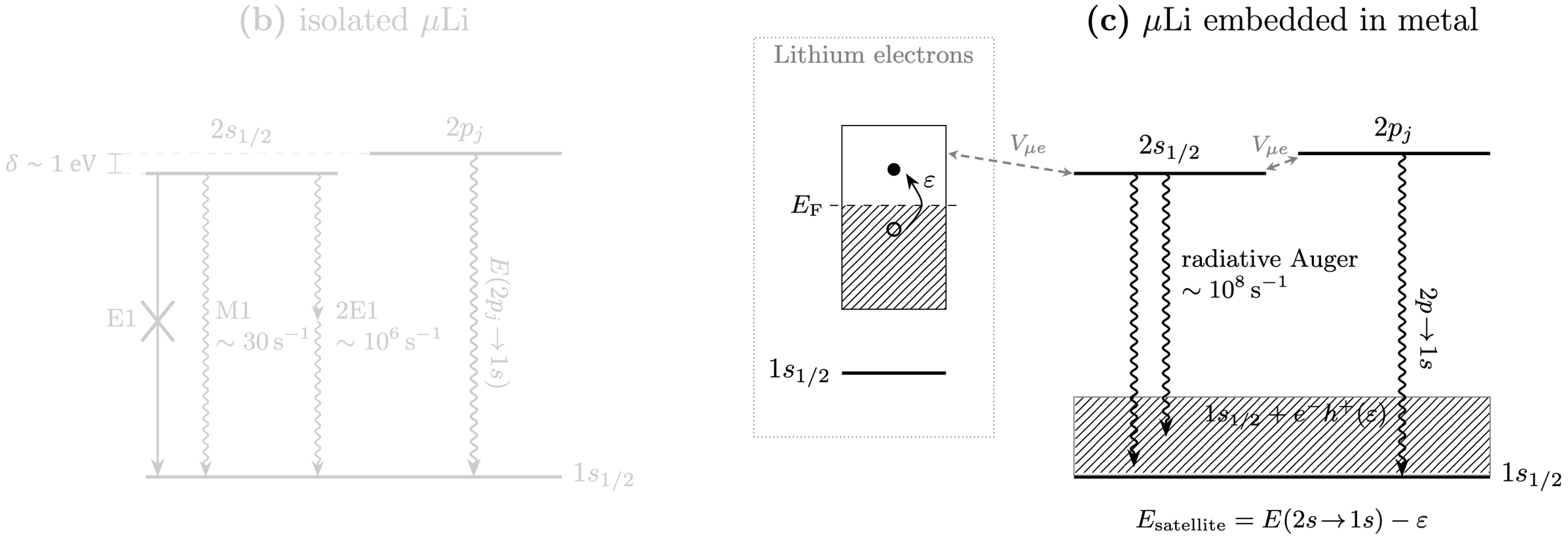

This has been identified as the dominant de-excitation mechanism for the 2s state of metallic, muonic lithium and described by Grechukhin & Soldatov in 1977 [5] but not yet observed and not much discussed in the literature.

Lithium 2p–1s transition with satellite

Using a phenomenological satellite model

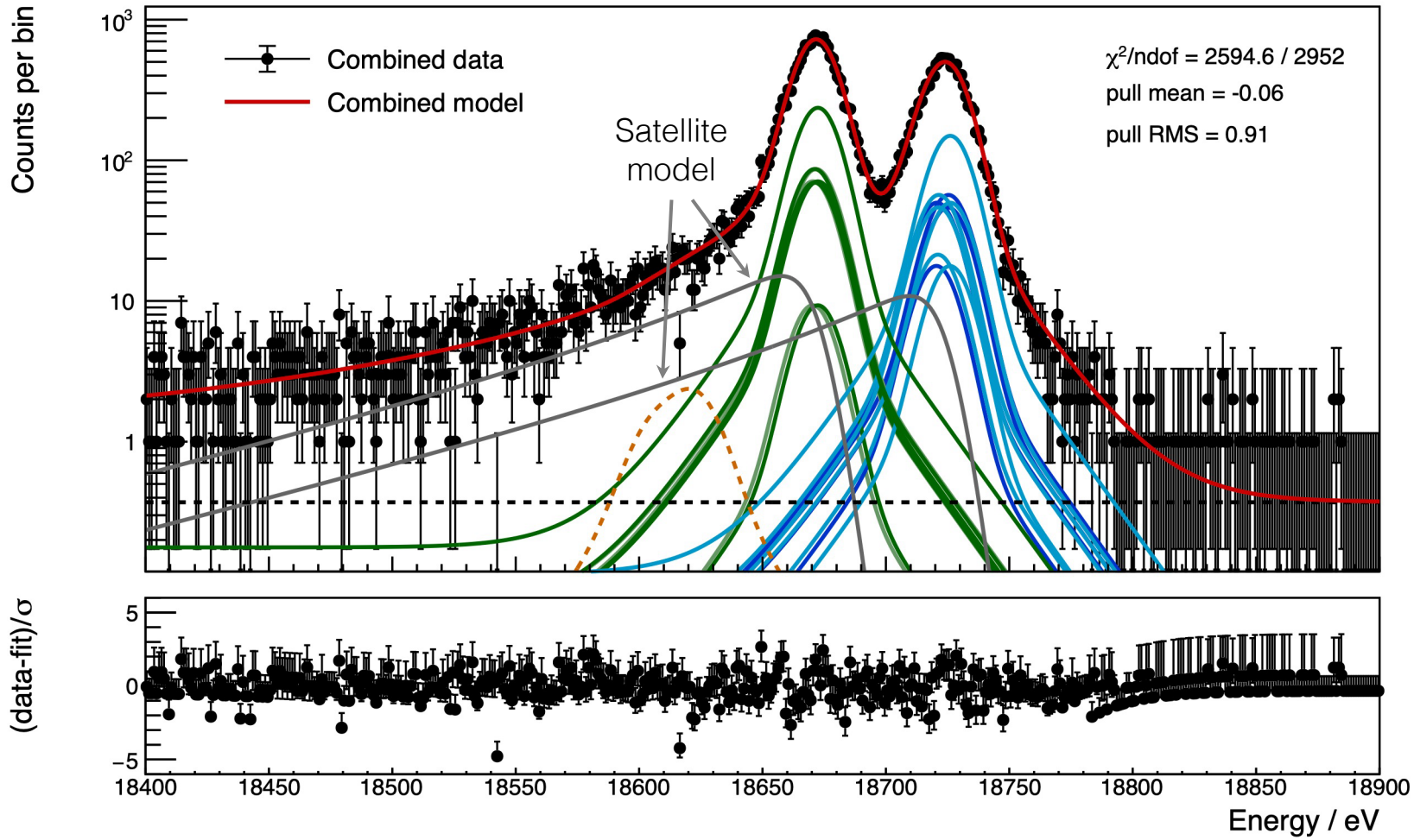

Lithium 2p–1s analysis strategy

A) Assume line shape problem
but no satellite

B) Assume 2s-1s satellite
but no line shape problem

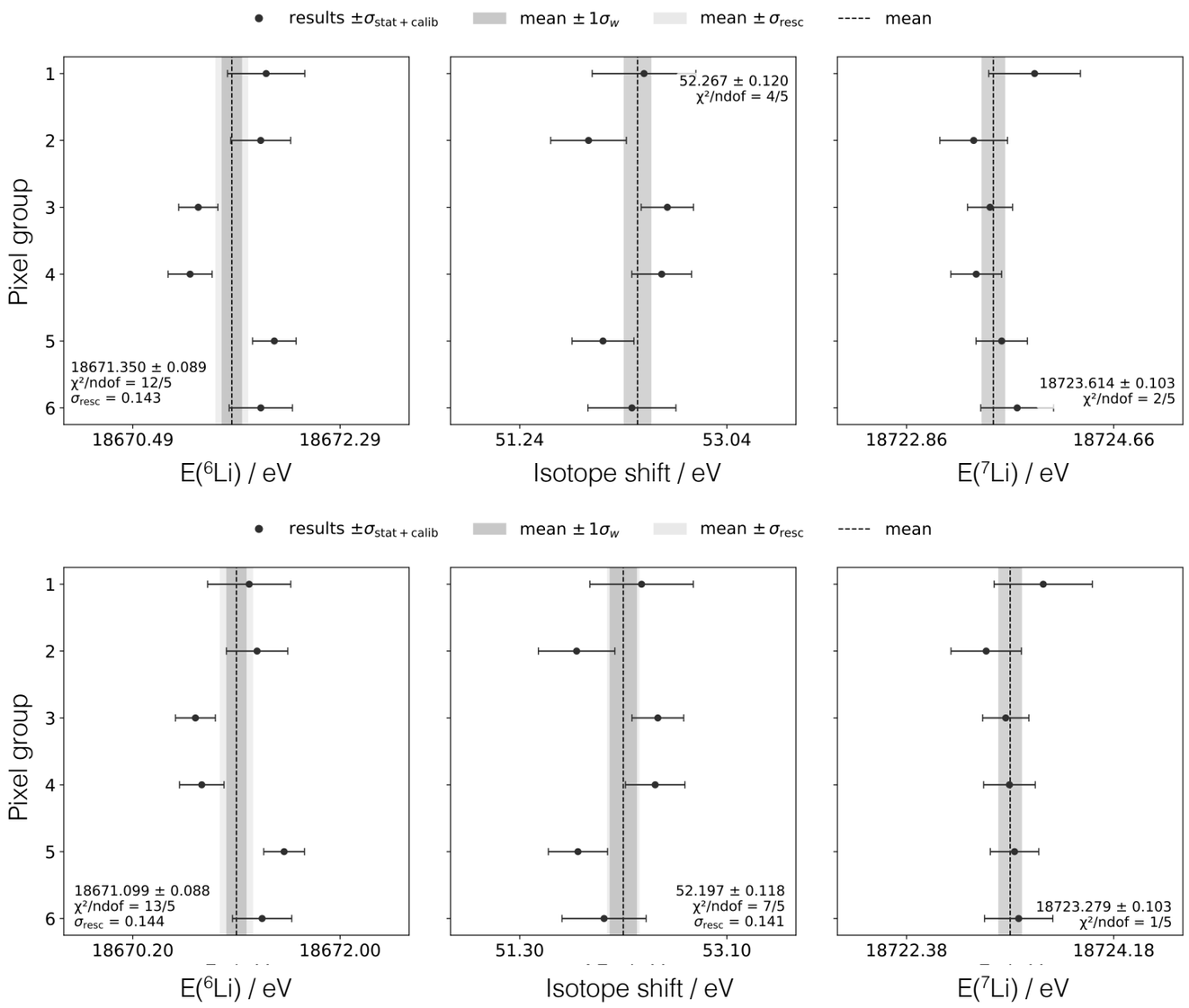

+ other systematics

Lithium 2p–1s results

		Energy / eV		
		^{6}Li	Isotope shift	^{7}Li
Nominal result	Weighted average	18671.230	52.232	18723.447
	Statistical uncertainty	0.088	0.118	0.103
Systematic uncertainty	Group inconsistency	0.114	0.077	0.000
	Calibration	0.018	0.002	0.018
	Pileup cut	0.055	0.137	0.128
	Line shape/satellite	0.142	0.085	0.217
	Time cut	0.011	0.007	0.017
	Binning	0.011	0.005	0.007
	Nb contamination	0.002	0.001	0.002
	Fit range	0.071	0.030	0.099
	Combined syst. uncertainty	0.204	0.181	0.272
Total uncertainty (syst. & stat.)		0.223	0.216	0.291

Energies are improved by 200-300 over existent values

⟹ low-energy tail represents dominant uncertainty in the 2p–1s energy measurement

Absolute nuclear charge radii of ^{6}Li and ^{7}Li

(*) Theory input and uncertainties are currently ongoing work by collaborators from JGU Mainz (see also: arXiv:2608.26988), TRIUMF, and HUJI

Direct extraction(*) from all μLi np-1s transitions measured in this work:

$$R(^6\mathrm{Li}) = 2.5771(84)\ \mathrm{fm}$$

$$R(^7\mathrm{Li}) = 2.4500(106)\ \mathrm{fm}$$

⟹ Factor 4-5 improvement over existing values

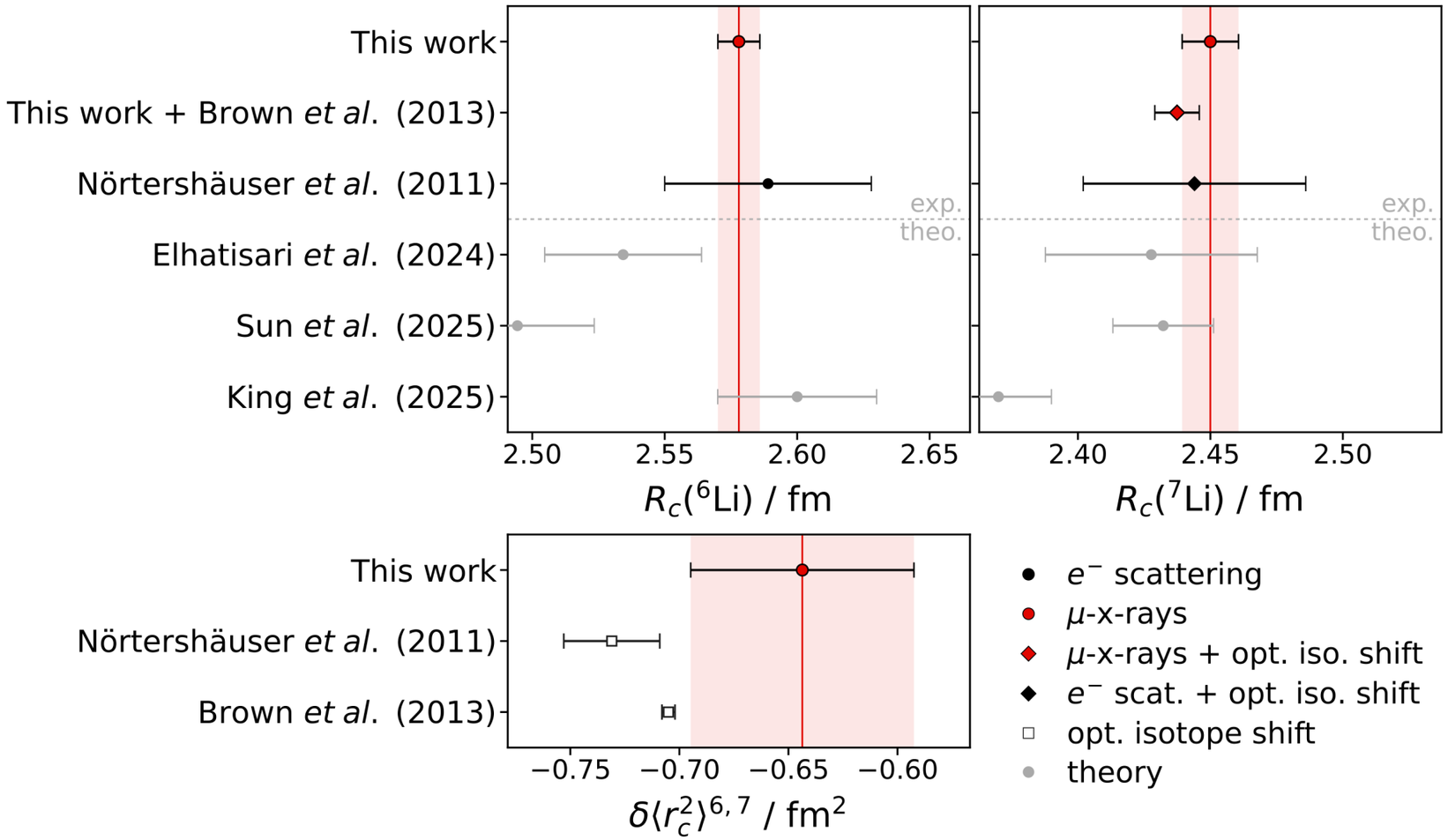

Closing the “radius gap”

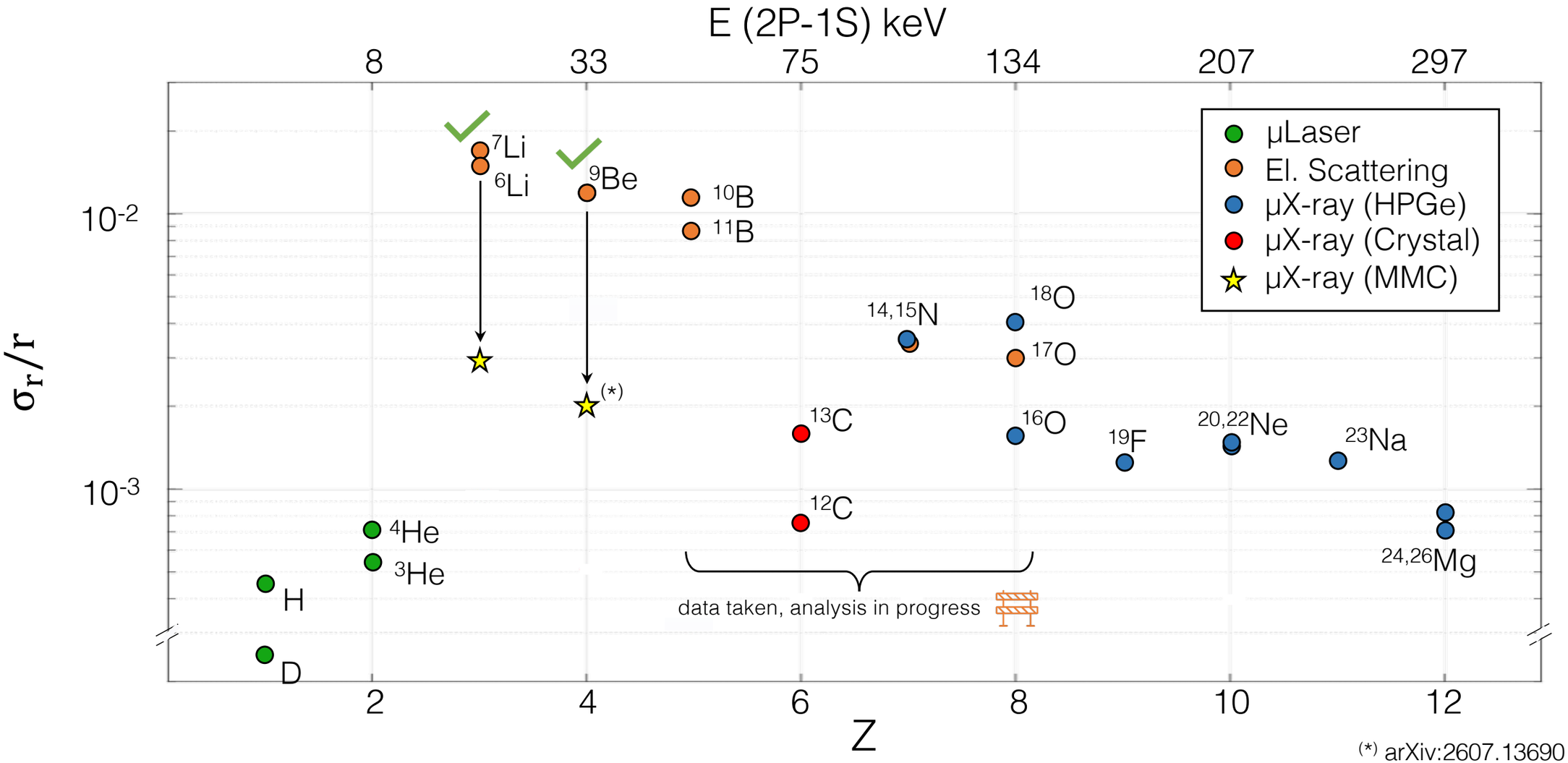

(*) arXiv:2607.13690

Conclusion and outlook

- ✓ Successful demonstration of MMCs as precision spectroscopy tool for low-energy muonic x-ray spectra
- ✓ Absolute nuclear charge radii of ^{6}Li and ^{7}Li were determined with substantial improvement to a relative precision of ~10^{-3}
  - → new precise benchmarks for ab-inito nuclear theory along the entire isotopic chain of lithium
- ✓ Improved energy resolution likely revealed a previously unresolved 2s-1s radiative-Auger satellite transition

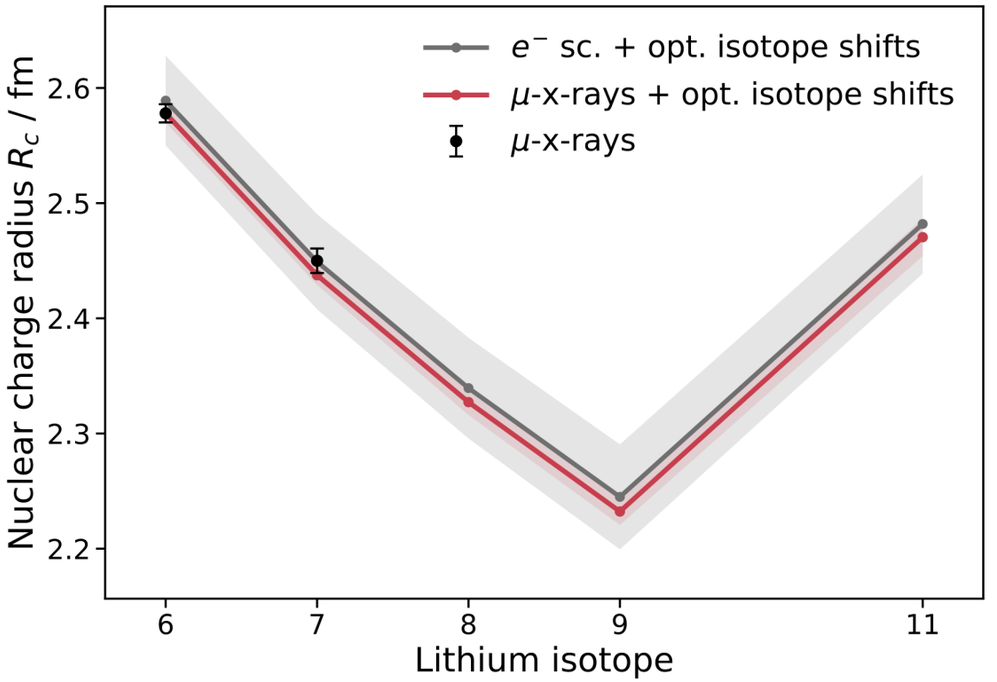

Next:

- ❒ Improve modelling of the satellite shape for further improvement of the charge radius measurement.
  - ❒ Ongoing work from groups at University of Warsaw and PSI
- ❒ Extend MMC-based x-ray spectroscopy to other light muonic atoms

A	$\delta\langle r^2\rangle^{6,A}$ / fm^2	R_c / fm
6	0	2.5780(79)
7	-0.705(3) [4]	2.4374(84)
8	-1.23(3) [3]	2.327(11)
9	-1.66(3) [3]	2.232(12)
11	-0.54(7) [3]	2.470(16)

Thank you for your attention!

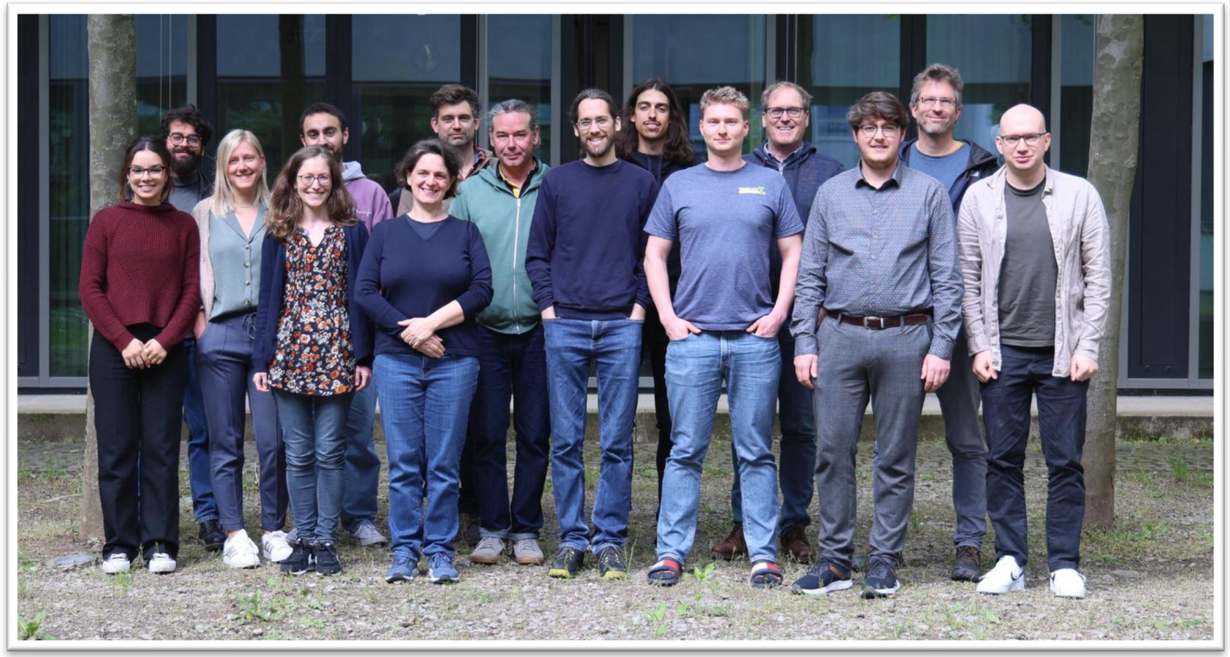

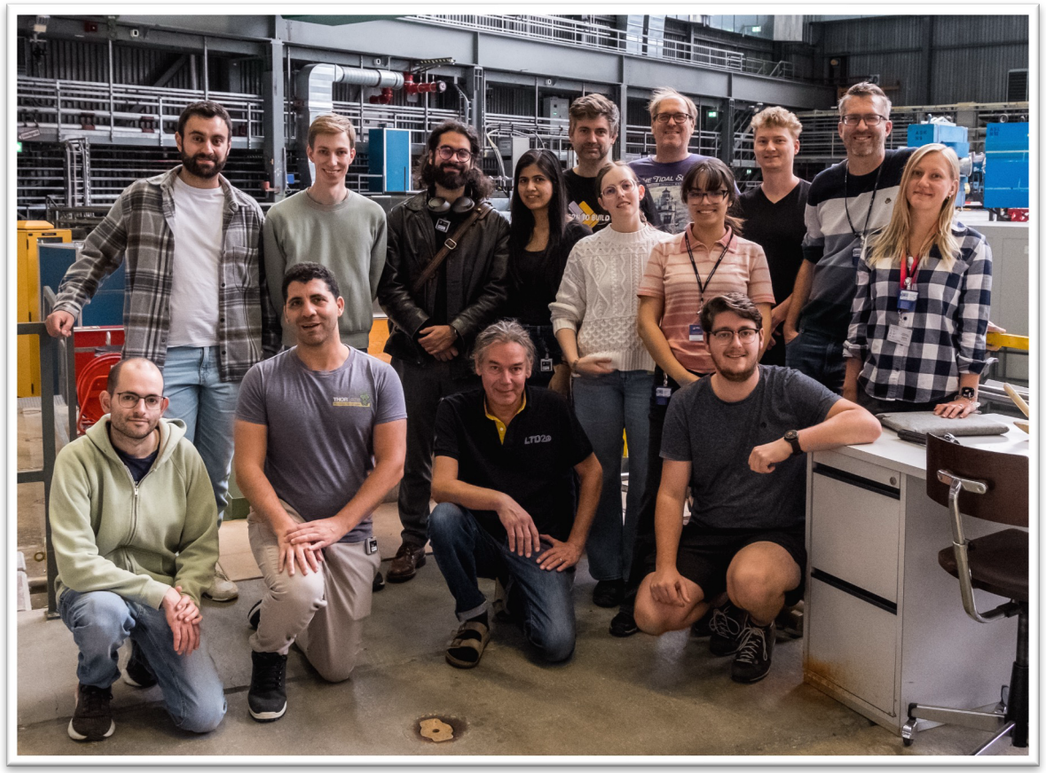

References

[1] W. Nörtershäuser et al., Charge radii and ground state structure of lithium isotopes: Experiment and theory reexamined, Phys. Rev. C 84, 024307 (2011), doi:10.1103/PhysRevC.84.024307.

[2] R. J. Harris et al., Energy and Width Measurements of Low-Z Pionic X-Ray Transitions, Phys. Rev. Lett. 20, 505 (1968), doi:10.1103/PhysRevLett.20.505.

[3] W. Nörtershäuser et al., Isotope-shift measurements of stable and short-lived lithium isotopes for nuclear-charge-radii determination, Phys. Rev. A 83, 012516 (2011), doi:10.1103/PhysRevA.83.012516.

[4] R. C. Brown et al., Quantum interference and light polarization effects in unresolvable atomic lines: Application to a precise measurement of the ^{6,7}Li D2 lines, Phys. Rev. A 87, 032504 (2013), doi:10.1103/PhysRevA.87.032504.

[5] D. Grechukhin and A. Soldatov, Effects impeding observation of weak neutral interaction between a muon and a nucleus in light mesic atoms, Zh. Eksp. Teor. Fiz 72, 390 (1977), https://jetp.ras.ru/cgi-bin/dn/e_045_02_0205.pdf.

Backup

Setup October 2024

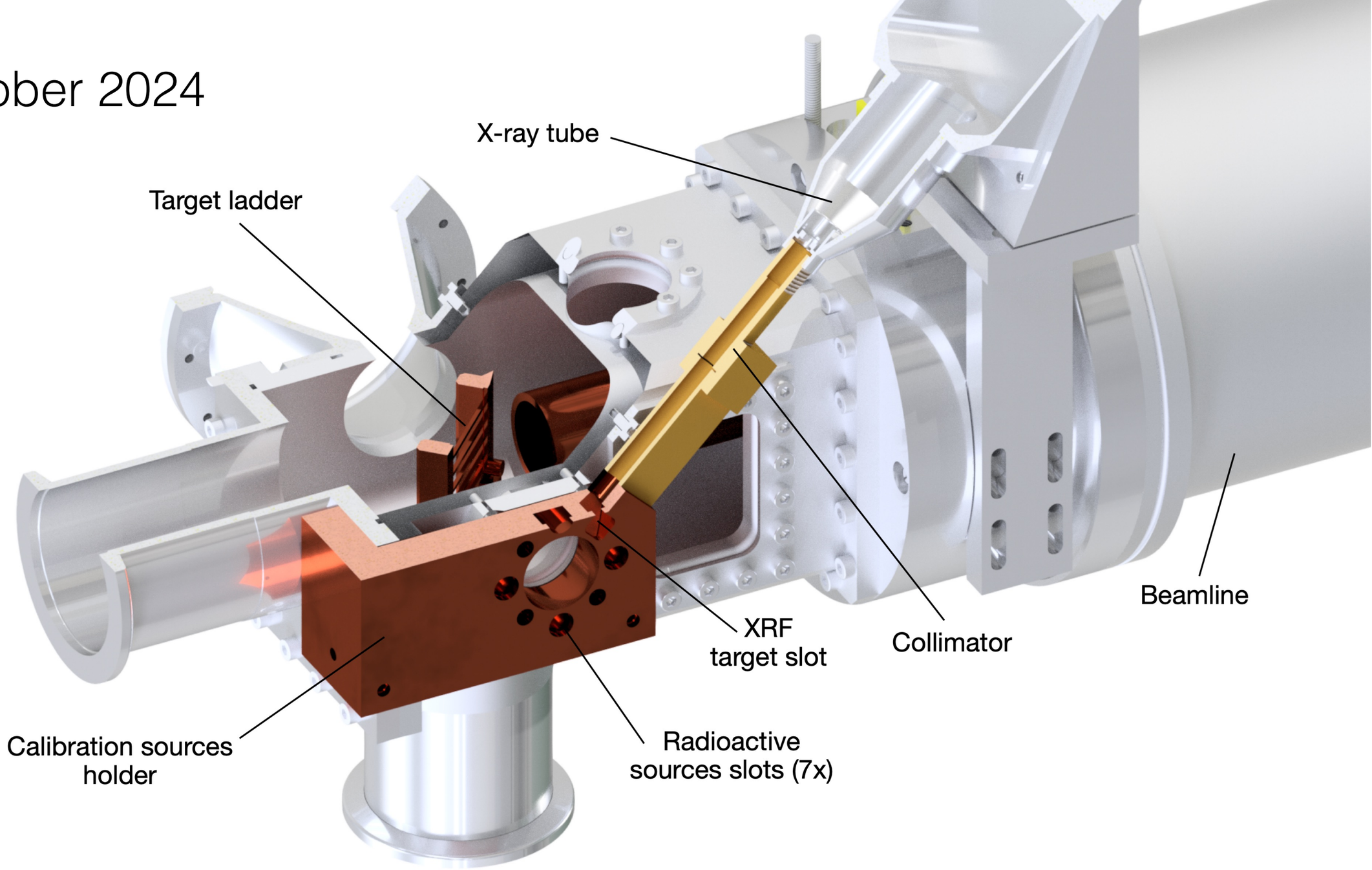

”maXs-30” MMC from Heidelberg

Detector design

Absorber pair wise coupled

→ Reduced sensitivity towards global temperature changes

→ (Reduced number of readout channels necessary)

Gradiometric design:

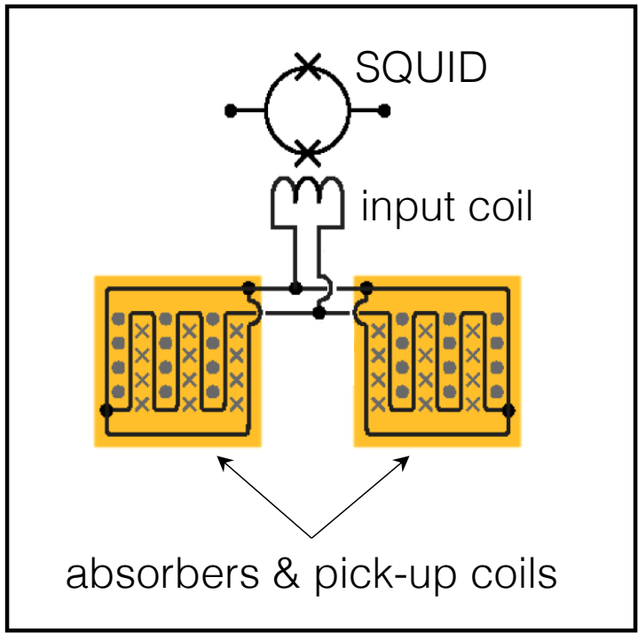

Temperature sensitive design:

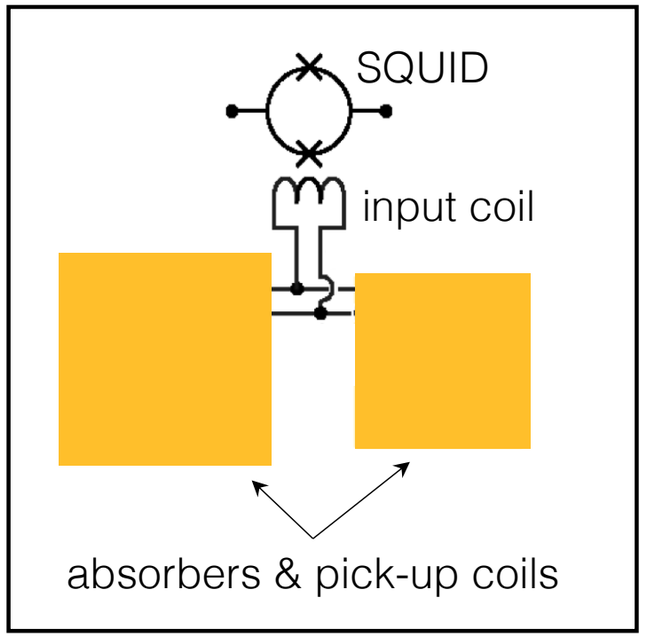

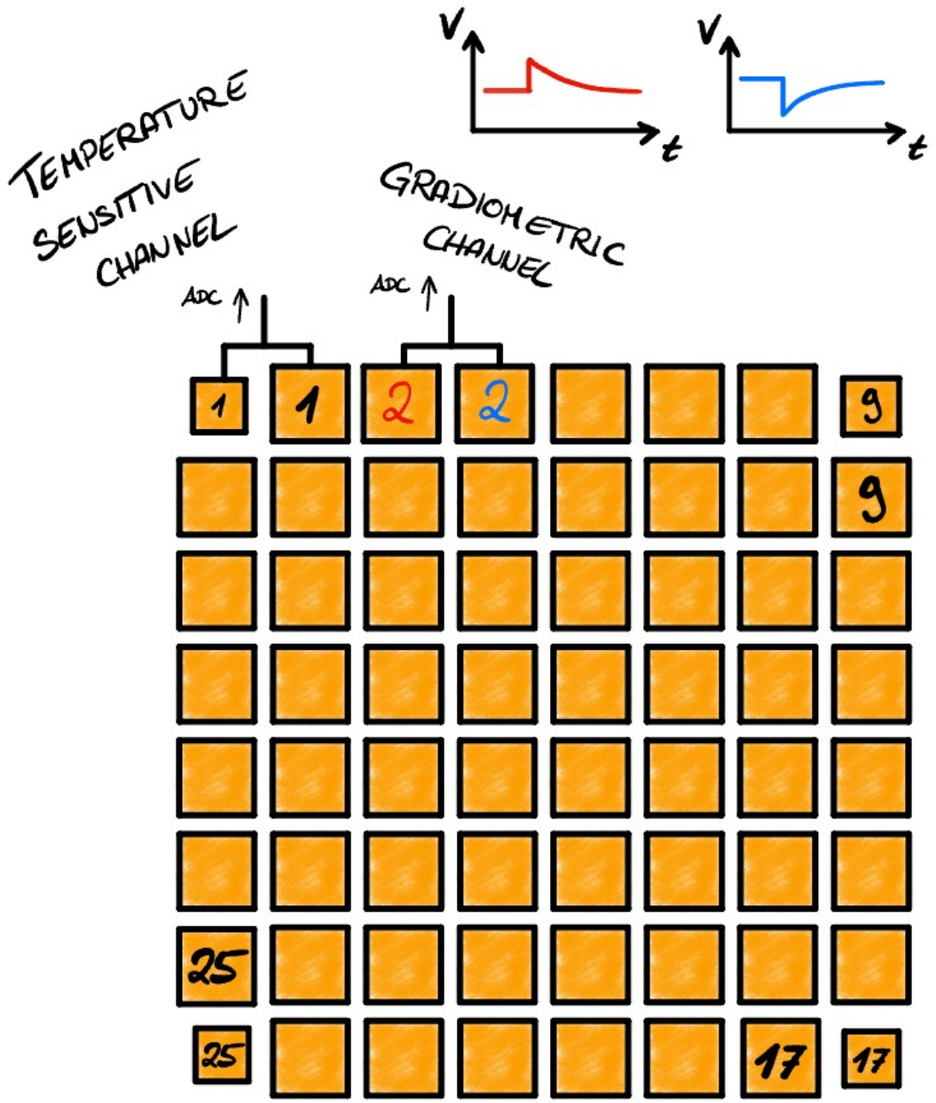

DOI: 10.1063/1.3292407

Data analysis workflow

Temperature correction

Temperature sensitive design:

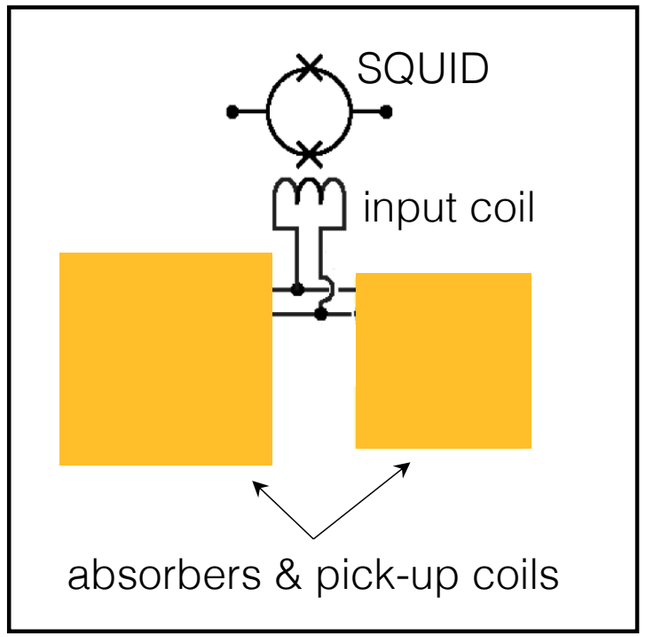

Triggered with every event

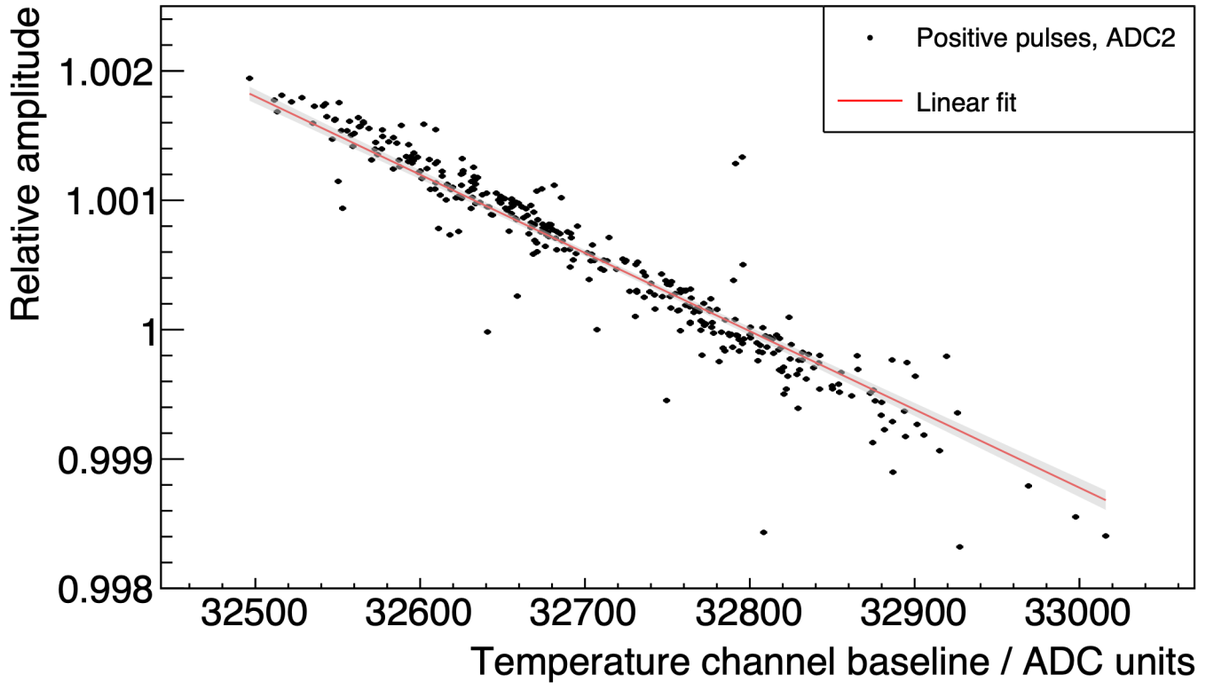

- Determine temperature sensitivity of gradiometric pixels and correct each event

ADC calibration

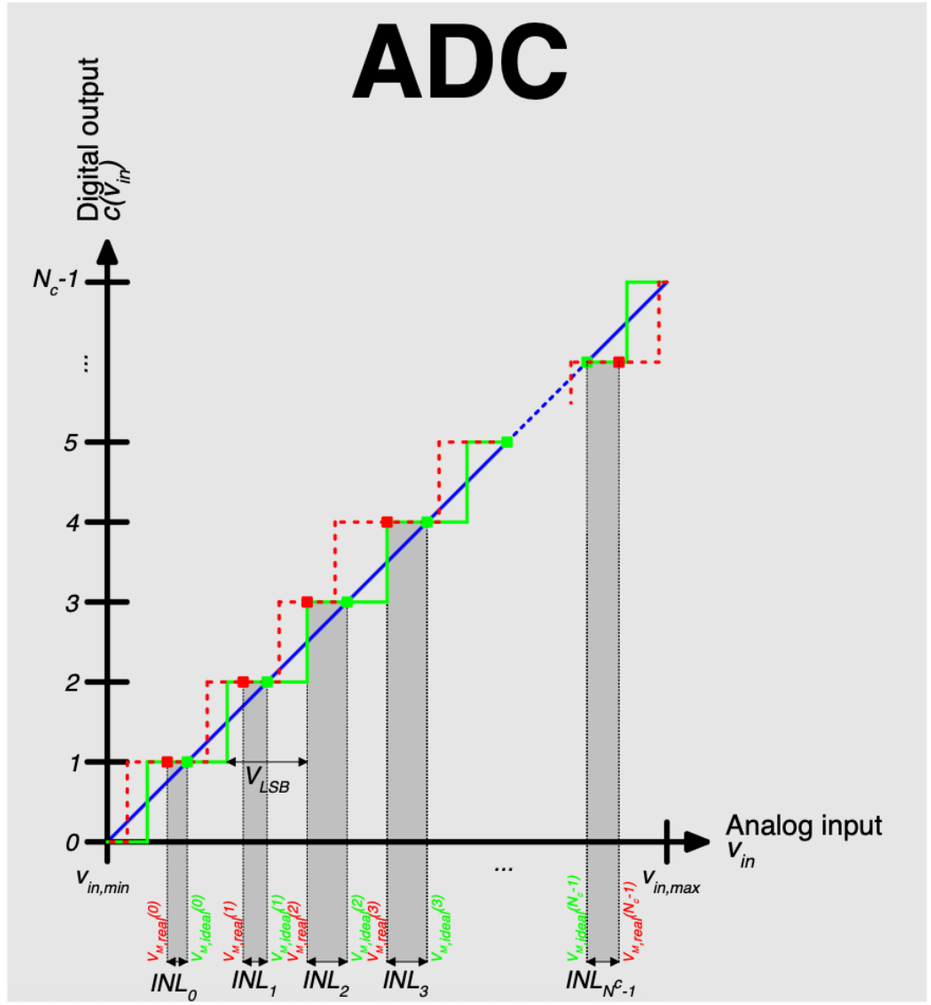

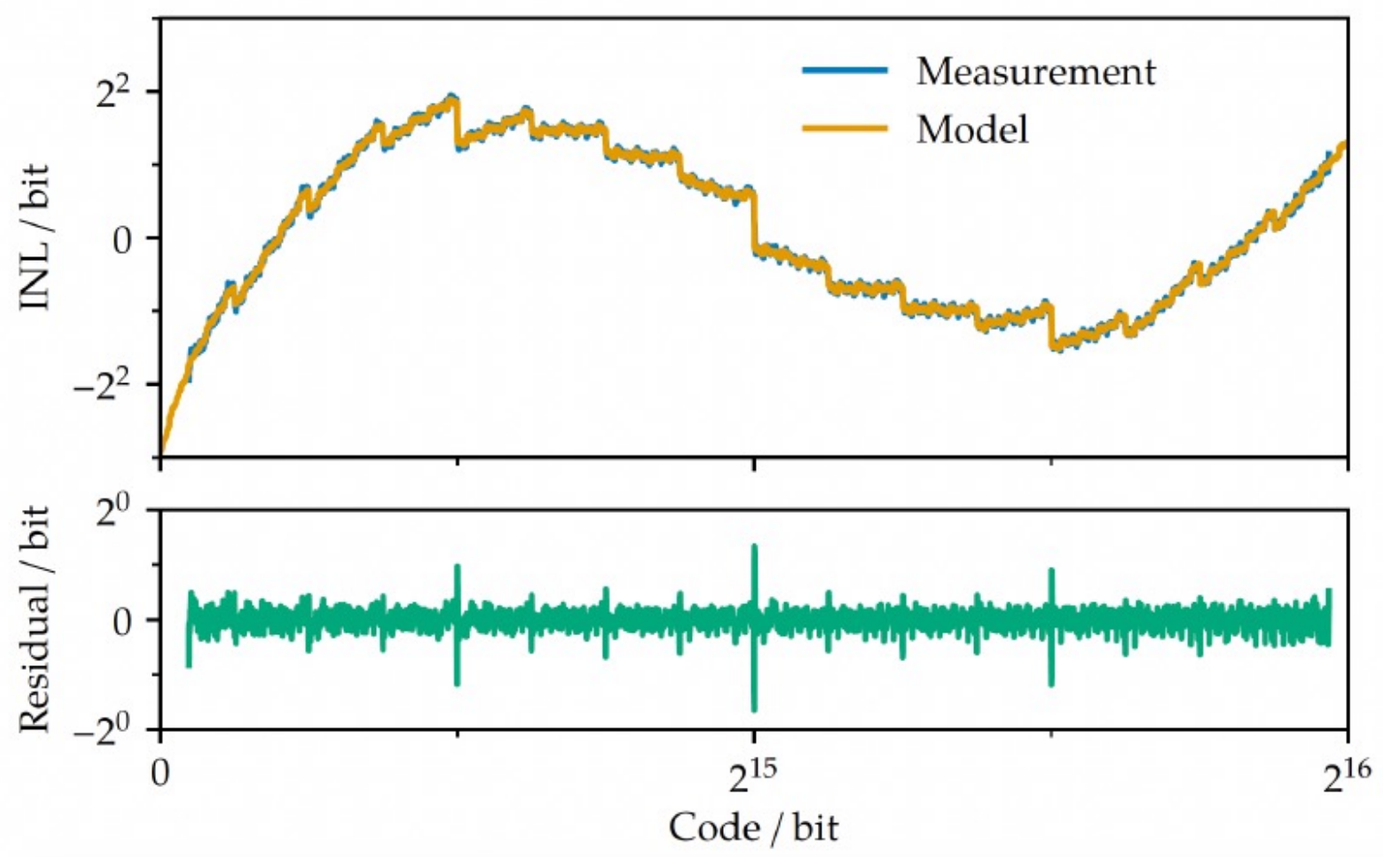

FIGURE 3.1: Example of a measured INL curve and the resulting bit-wise calibration function for a single ADC channel. Figure taken from D. Unger [130].

Data analysis workflow

Background identification

(1) “good“ photon events

(2) Decay electron energy deposition in absorber

(3) (mostly) low-energy co-triggered pulses

(4) Athermal phonons originating from substrate

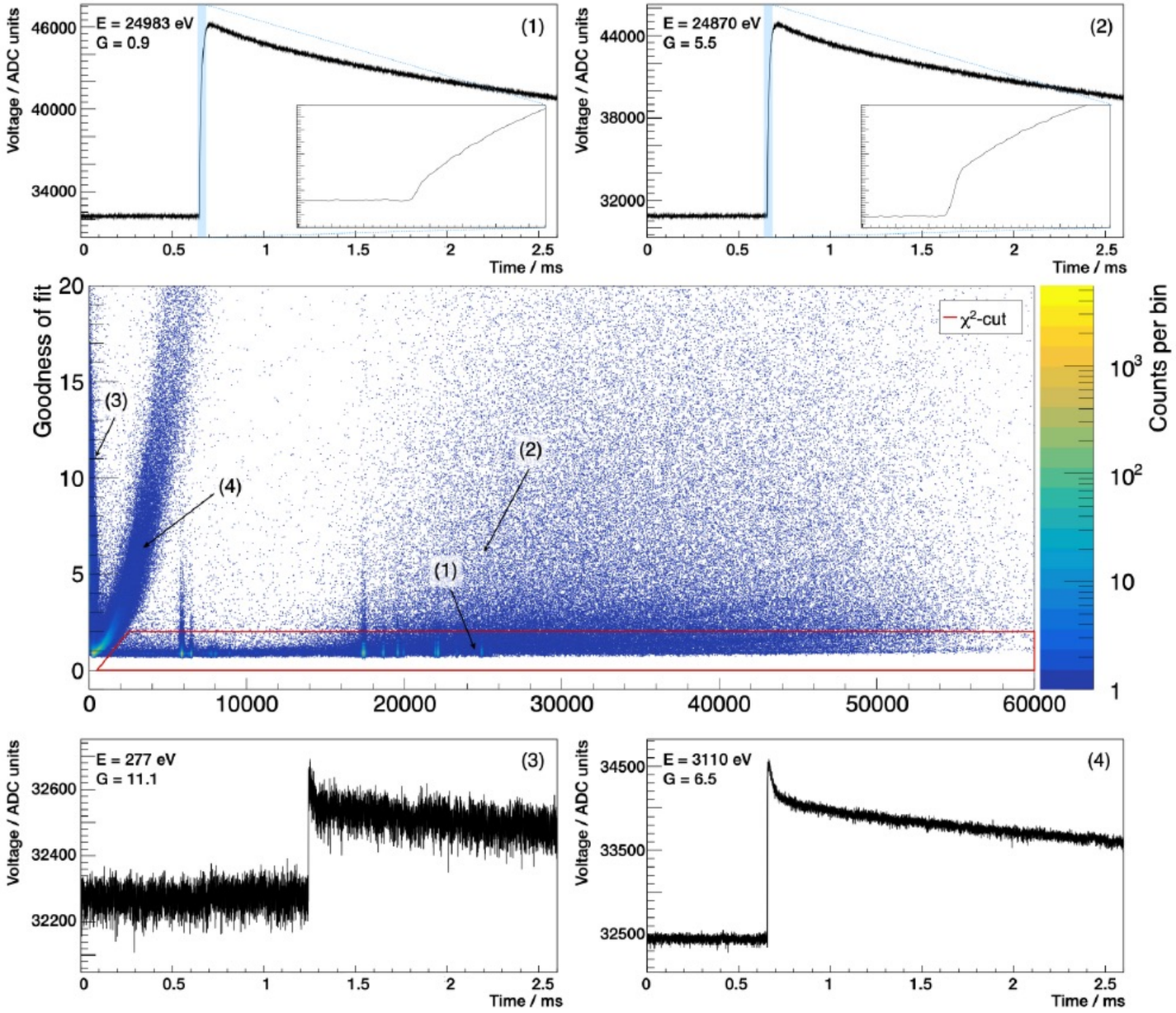

Data analysis workflow

Background identification

Spatial distribution of coincident triggers on the detector e.g.:

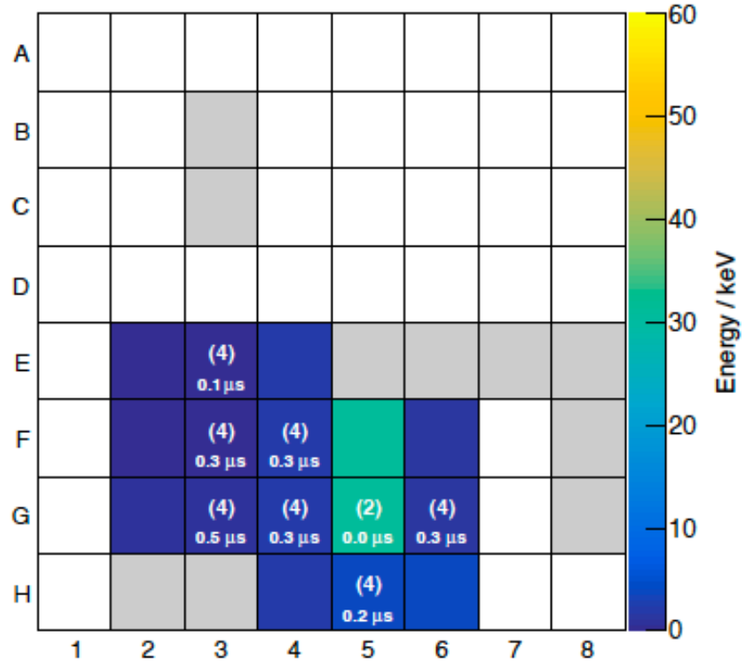

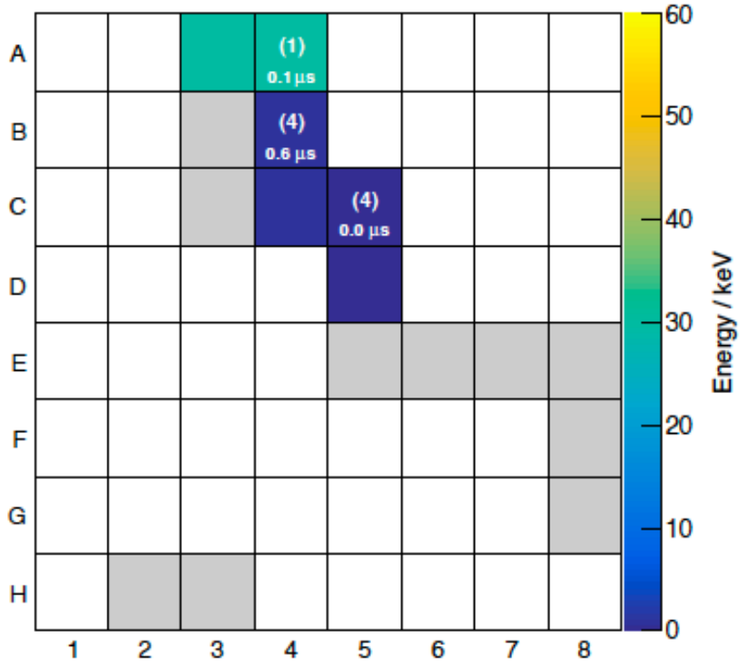

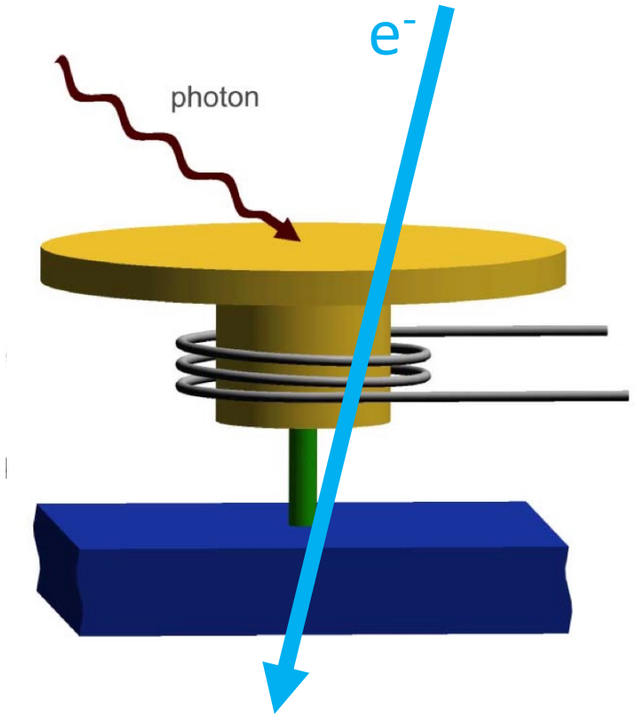

Michel electrons shoot through absorbers into silicon substrate and heat-up pixels “from the backside”

Decay electron effect on detector performance

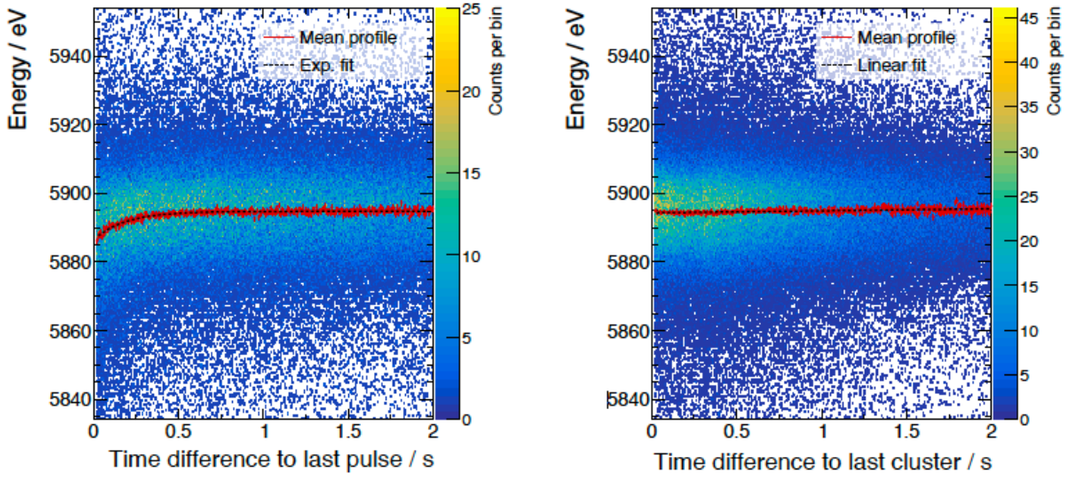

(a) Mn K$\alpha_{1,2}$

(b) Mn K$\alpha_{1,2}$

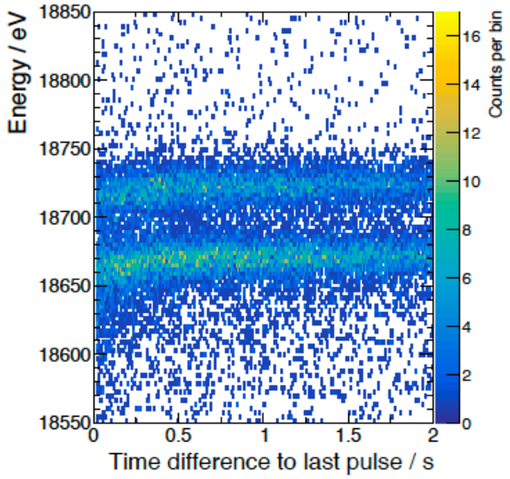

(c) μLi 2p$\rightarrow$1s

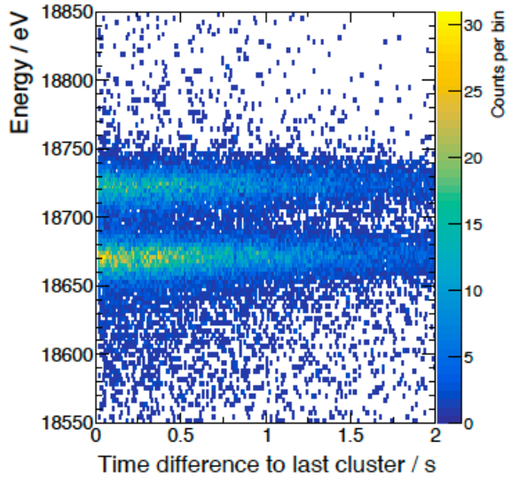

(d) μLi 2p$\rightarrow$1s

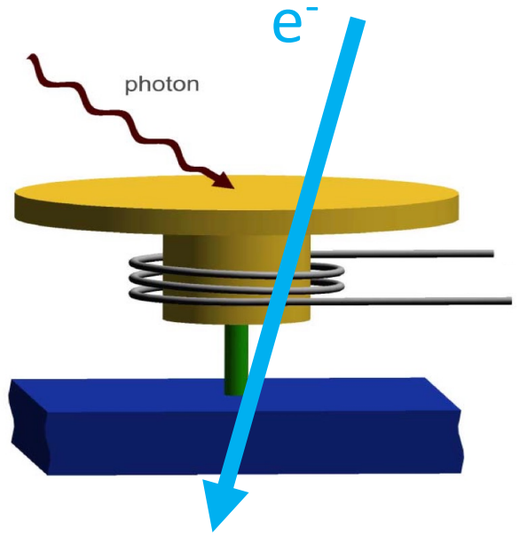

Gradiometric design:

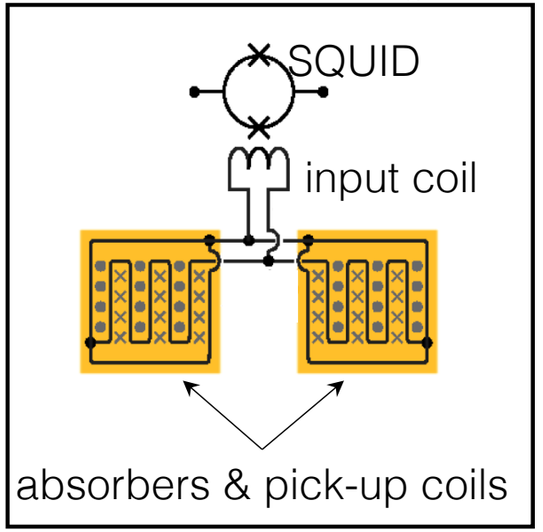

DOI: 10.1063/1.3292407

Background contributions

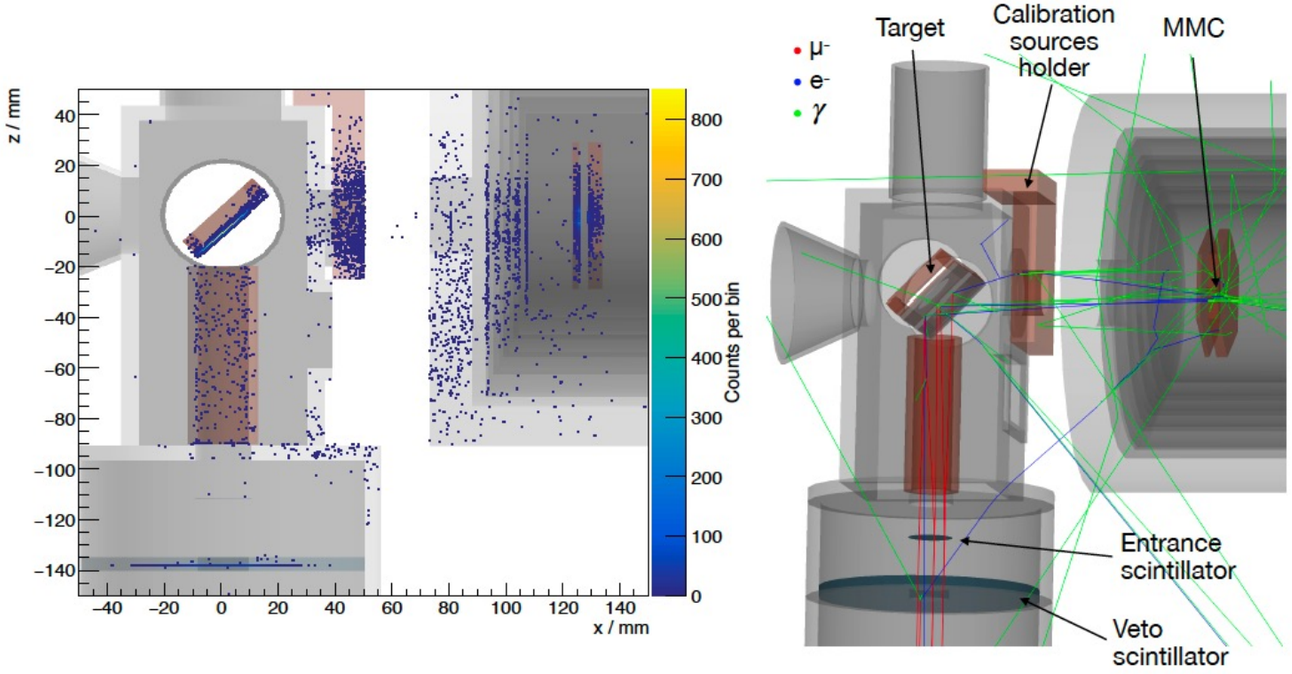

FIGURE B.1: Geant4 background simulation results, showing the origin of events detected on the MMC. The origin of Michel electrons lies largely in the veto scintillator and the target. In a muon coincidence cut using the entrance scintillator, events from the veto and those within the MMC shielding along the connecting axis are excluded. X-ray fluorescence comes almost exclusively from the MMC holder and the collimator, while delta electrons originate from all the material along the axis connecting the target and the MMCs. The calibration sources holder is the strongest source of bremsstrahlung.

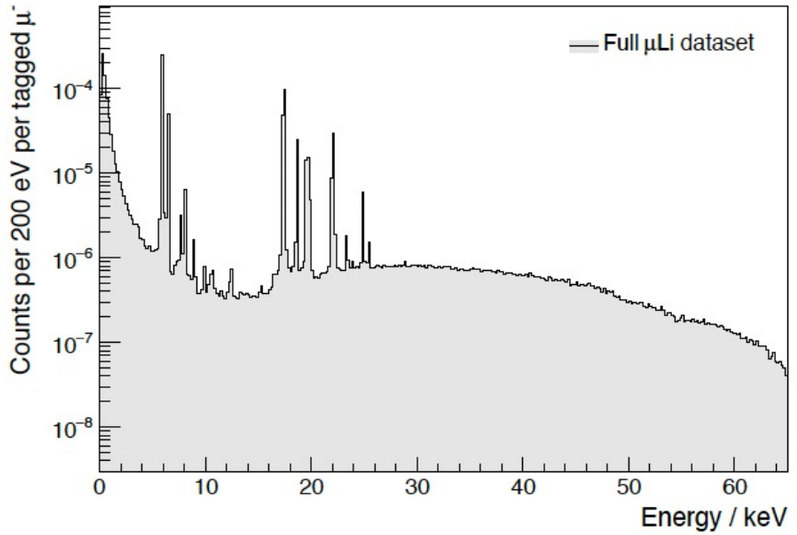

(a) Experimental spectrum

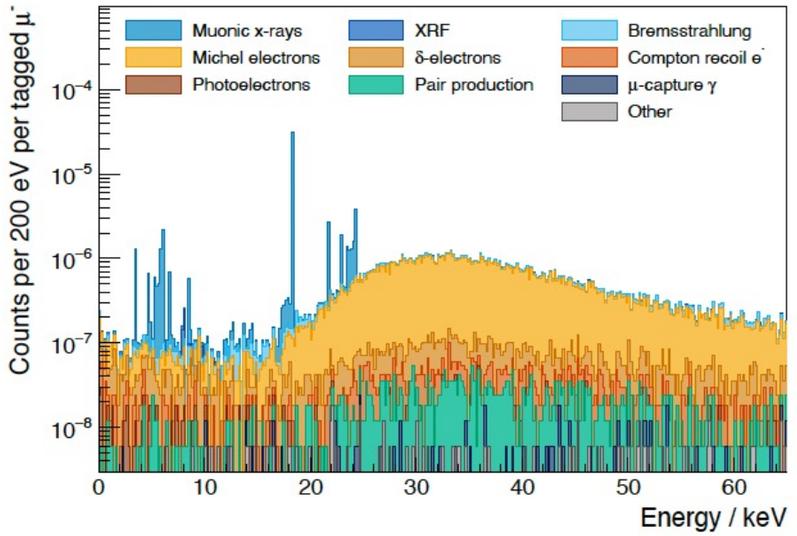

(b) Simulated spectrum

Lithium 3p-1s & 4p-1s energies

TABLE 4.8: Results of the measured μ^6Li and μ^7Li $3p_{1/2} \rightarrow 1s_{1/2}$ and $4p_{1/2} \rightarrow 1s_{1/2}$ x-ray energies as well as the respective isotope shifts. The nominal fit uses the calibration-derived fixed line shape.

		$3p_{1/2} \rightarrow 1s_{1/2}$			$4p_{1/2} \rightarrow 1s_{1/2}$		
		E_6 / eV	ΔE_{IS} / eV	E_7 / eV	E_6 / eV	ΔE_{IS} / eV	E_7 / eV
Nominal result	Weighted average	22124.405	61.189	22185.594	23332.263	64.774	23397.048
	Statistical unc.	0.148	0.231	0.189	0.379	0.583	0.453
Systematic uncertainty	Group inconsistency	0.000	0.000	0.181	0.000	0.000	0.000
	Calibration	0.023	0.003	0.022	0.022	0.010	0.020
	Pileup cut	0.080	0.124	0.073	0.180	0.349	0.173
	Line shape	0.067	0.050	0.015	0.677	0.004	0.640
	Time cut	0.067	0.051	0.099	0.059	0.050	0.067
	Binning	0.005	0.007	0.008	0.013	0.032	0.029
	Fit range	0.001	0.006	0.005	0.041	0.017	0.055
	Combined syst. unc.	0.126	0.143	0.220	0.705	0.355	0.670
Total unc. (syst. & stat.)		0.195	0.272	0.291	0.800	0.682	0.808

Radius extraction model

Model: $E(R_c) = E_0 + k_2 (R_c^2 - R_0^2) + k_3 (R_c^3 - R_0^3) + \delta E_{ES} + \delta E_{NP}$

Radius sensitivity: $k_2(^6\mathrm{Li}) = -4.424\ \mathrm{eV/fm^2}$, $k_3(^6\mathrm{Li}) = 0.083\ \mathrm{eV/fm^3}$,
$k_2(^7\mathrm{Li}) = -4.458\ \mathrm{eV/fm^2}$, $k_3(^7\mathrm{Li}) = 0.084\ \mathrm{eV/fm^3}$

TABLE 4.13: Parametrization offsets E_0 computed with the MDFGME code [120] and electron screening shifts ΔE_{ES} between zero and two electrons in the 1s orbital, obtained using mudirac [59]. The nominal electron screening correction applied is $\delta E_{ES} = \Delta E_{ES}/2$, with a symmetric uncertainty $\sigma_{ES} = |\delta E_{ES}|$.

	μ^6Li		μ^7Li	
Transition	E_0 / eV	ΔE_{ES} / eV	E_0 / eV	ΔE_{ES} / eV
$2p_{1/2} \rightarrow 1s_{1/2}$	18670.651(14)	−0.021	18722.993(14)	−0.021
$3p_{1/2} \rightarrow 1s_{1/2}$	22124.215(14)	−0.132	22185.710(14)	−0.131
$4p_{1/2} \rightarrow 1s_{1/2}$	23332.741(14)	−0.427	23397.438(14)	−0.425

Nuclear polarization: $\delta E_{NP}(\mu^6\mathrm{Li}) = 191(57)$ meV, $\delta E_{NP}(\mu^7\mathrm{Li}) = 258(77)$ meV

Radius extraction results

TABLE 4.14: Absolute nuclear charge radii of ^{6}Li and ^{7}Li extracted from the three np $\rightarrow$ 1s transitions, with a breakdown of the uncertainty contributions originating from the experimental energy measurement and the theoretical modeling.

		$R_c(\mu^6\mathrm{Li})$/fm			$R_c(\mu^7\mathrm{Li})$/fm		
		2p $\rightarrow$ 1s	3p $\rightarrow$ 1s	4p $\rightarrow$ 1s	2p $\rightarrow$ 1s	3p $\rightarrow$ 1s	4p $\rightarrow$ 1s
Nominal result		2.568 7	2.583 9	2.608 1	2.437 5	2.462 3	2.468 3
Experimental unc.	Energy measurement	0.010 6	0.009 2	0.037 4	0.013 4	0.014 2	0.039 6
	Electron screening	0.000 5	0.003 1	0.010 0	0.000 5	0.003 2	0.010 4
Theory unc.	Nuclear polarization	0.002 7	0.002 7	0.002 7	0.003 8	0.003 8	0.003 8
	QED corrections	0.000 5	0.000 5	0.000 5	0.000 5	0.000 5	0.000 5
	Charge distribution model	0.002 4	0.002 4	0.002 3	0.002 5	0.002 4	0.002 4
Total uncertainty		0.011 2	0.010 4	0.038 9	0.014 2	0.015 3	0.041 2

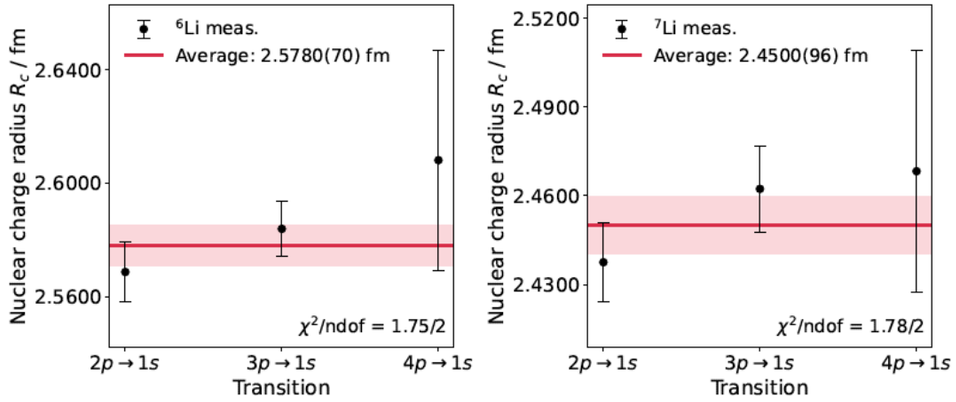

Averaged final result:

$$R_c(^6\mathrm{Li}) = 2.5780(70)_{\mathrm{exp}}(36)_{\mathrm{theo}}\ \mathrm{fm}\,,$$
$$R_c(^7\mathrm{Li}) = 2.4500(96)_{\mathrm{exp}}(46)_{\mathrm{theo}}\ \mathrm{fm}\,.$$
$$\delta\langle r_c^2\rangle^{6,7} = -0.644(42)_{\mathrm{exp}}(29)_{\mathrm{theo}}\ \mathrm{fm}^2\,.$$

Intensities and lithium cascade

TABLE 4.10: Relative Lyman-series intensities measured in this work, compared with previous measurements and the best-fitting cascade calculation using $\alpha = 0.06$, $K_{WD} = 10\,eV$ and initial principal quantum number n = 14.

	$I/I_{2p\to1s}$			
Line	This work	Ref. [206]	Ref. [207]	Calculation
2p → 1s	1	1	1	1
3p → 1s	0.353(4)	0.374(11)	0.356(10)	0.319
4p → 1s	0.057 4(16)	0.061 9(19)	0.051(3)	0.065 3
5p → 1s	0.006 4(8)	0.006 4(7)	0.005 6(3)	0.008 49

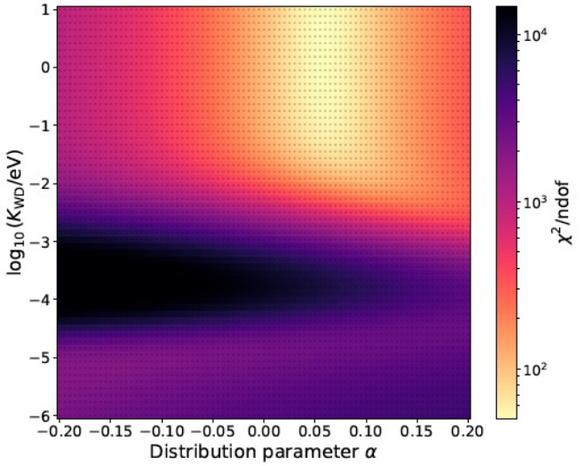

(a) Goodness of fit for the sampled parameter space.

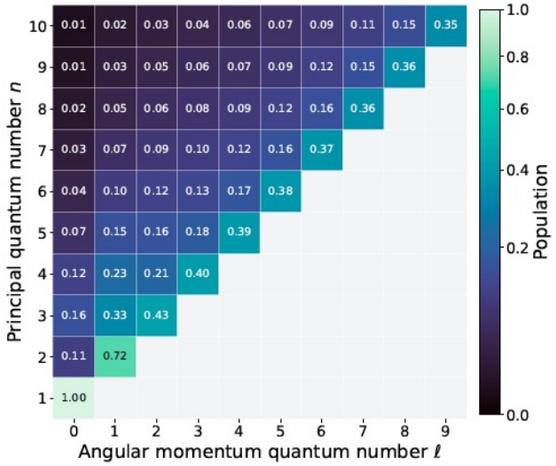

(b) Calculated cascade populations for the best-fitting parameter combination.

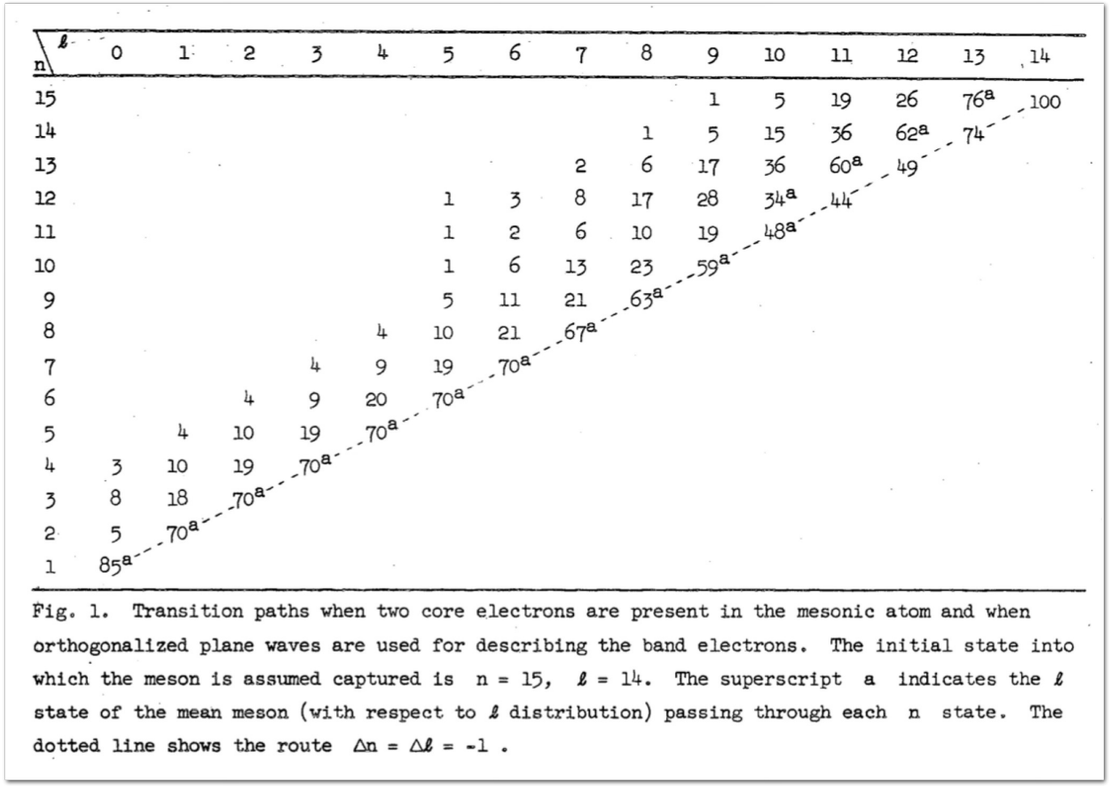

Fig. 1. Transition paths when two core electrons are present in the mesonic atom and when orthogonalized plane waves are used for describing the band electrons. The initial state into which the meson is assumed captured is n = 15, ℓ = 14. The superscript a indicates the ℓ state of the mean meson (with respect to ℓ distribution) passing through each n state. The dotted line shows the route Δn = Δℓ = -1 .

C. R. Johnson, Transition Paths of μ− Mesons Captured in Solid Lithium, Ph.D. thesis, University of California, Berkeley, Lawrence Radiation Laboratory Report No. UCRL-10965 (1963), https://escholarship.org/uc/item/28z2t331.